Final published version of this article: **The Journal of Physical Chemistry C**,
Cite this: *J. Phys. Chem. C* 2022, 126, 5, 2548−2560
Publication Date:January 27, 2022

https://doi.org/10.1021/acs.jpcc.1c09776

Trimethylamine Probes Isolated Silicon Dangling Bonds and Surface Hydroxyls of (H,OH)-Si(001)

Lucía Pérez Ramírez[1†‡], Niklas Fornefeld[2‡], Fabrice Bournel[1,3], Stefan Kubsky[3], Elena Magnano[4,5] Federica Bondino[4], Ulrich Köhler[2], Stéphane Carniato[1], Jean-Jacques Gallet[1,3] and François Rochet[1*]*

[1] Sorbonne Université, CNRS, Laboratoire de Chimie Physique matière et Rayonnement, UMR 7614, 4 place Jussieu, 75005 Paris, France

[2] Fakultät für Physik und Astronomie, Institut für Experimentalphysik IV AG Oberflächenphysik, Ruhr-Universität Bochum, D-44780 Bochum, Germany [3] Synchrotron SOLEIL, L'Orme des Merisiers, Saint-Aubin - BP 4891192 Gif-sur-Yvette CEDEX, France

[4] IOM-CNR, Laboratorio TASC, 34149 Basovizza, Trieste, Italy

[5] Department of Physics, University of Johannesburg, PO Box 524, Auckland Park 2006, South Africa

KEYWORDS: silicon surface, adsorption, reaction, amine, water, hydrogen bond, silicon dangling bond

ABSTRACT. The water-terminated Si(001) surface, (H,OH)-Si(001), covered with hydroxyls and hydrides, is both a model surface for adsorption studies and a promising starting substrate for area selective atomic layer deposition. A motivation of the present work was to advance an understanding of why amines catalyze the reactivity of SiOH with silanes. Combining real-time

synchrotron radiation X-ray photoelectron spectroscopy (XPS) and high-resolution electron energy loss spectroscopy (HREELS) with quantum chemistry DFT calculations of core-level ionization energies and vibrational spectra, we determined the bonding configurations of trimethylamine on (H,OH)-Si(001) at cryogenic temperatures, under pressures in the 10^{-9} - 10^{-8} mbar range. Both XPS and HREELS show that the majority species are trimethylamine molecules making acceptor H bonds with surface hydroxyls. Moreover, HREELS indicate that the hydrogen-bonding modes (interpreted as single and double proton acceptor bonds) depend on temperature and/or coverage, which may in turn affect the weakening the O-H bond, and hence the catalytic effects of trimethylamine. XPS also clearly detects a minority species, trimethylamine datively bonded to the isolated silicon dangling bonds remaining on the surface (a few $1/100^{th}$ of a monolayer) after water saturation. This species is prone to breaking, and a detailed analysis of the reaction products is given. Possible mechanisms leading to decomposition (including beam damage) are also discussed. In any case, the reactivity of the isolated silicon dangling bonds with the amine may impact the density of surface/interface electrically active defects and hence band bending, a vital question when oxide/silicon interfaces are formed.

1. Introduction

The water-terminated Si(001) surface, denoted (H,OH)-Si(001), that results from the dissociative adsorption of water[1,2,3,4] on the clean dimerized surface, is a model surface to study molecular interactions and reactions with surface hydroxyls.[5–7] This is because the H/OH surface patterns (see Figure 1) are well known as they are directly visualized in scanning tunneling microscopy images.[1,2,3,6] This is obviously impossible for hydroxylated silica surfaces because

SiO_2 is insulating. (H,OH)-Si(001) is also a nearly perfect passivated surface, with isolated silicon dangling bonds (IDBs) amounting to a few 10^{-2} silicon monolayer (ML).[3,4]

Viewed from a more applied perspective, (H,OH)-Si(001) can also be the right starting surface for the atomic layer deposition (ALD) of high-κ oxides (HKO) on Si(001).[8,9] There would be some advantages to start the HKO growth *directly* from the silicon substrate. In fact, the presence of an interfacial layer of SiO_2 in between the HKO/Si stack limits the highest possible gate stack capacitance.[10] Moreover, starting from (H,OH)-Si(001), the electrically active surface defects, the IDBs, are accessible to molecules (including organic ones) that could passivate them (see refs.[6,11]). The (H,OH)-Si(001) surface could also be suitable for area selective ALD (ASD), as it could be alkylated via the reaction of an aminosilane with an hydroxyl. In fact, in ASD processes OH-covered SiO_2 and TiO_2 surfaces are commonly exposed to dimethylaminotrimethylsilane[12,13] to be terminated with $-OSi(CH_3)_3$ units, that inhibit the ALD growth of oxides.

A fundamental surface chemistry issue raised by the ALD of oxide layers is the reactivity of surface hydroxyls with metal complexes and silanes. In particular, ammonia and amines have a proven catalytic effect on the reactivity of surface OH with chloro- and alkoxysilanes.[14,15,16,17,18] It has been argued that a strong basicity of the amine boosts the catalytic efficiency, as the adsorbed molecule makes an acceptor H bond with the hydroxyl, which in turn weakens the O–H bond.[19] Similarly, the reaction path of an aminosilane (in an ASD process) also requires the activation of the O-H bond. This involves the formation of a strong hydrogen bond between the amino nitrogen and the hydroxyl. This type of reaction is therefore considered as autocatalyzed.[20]

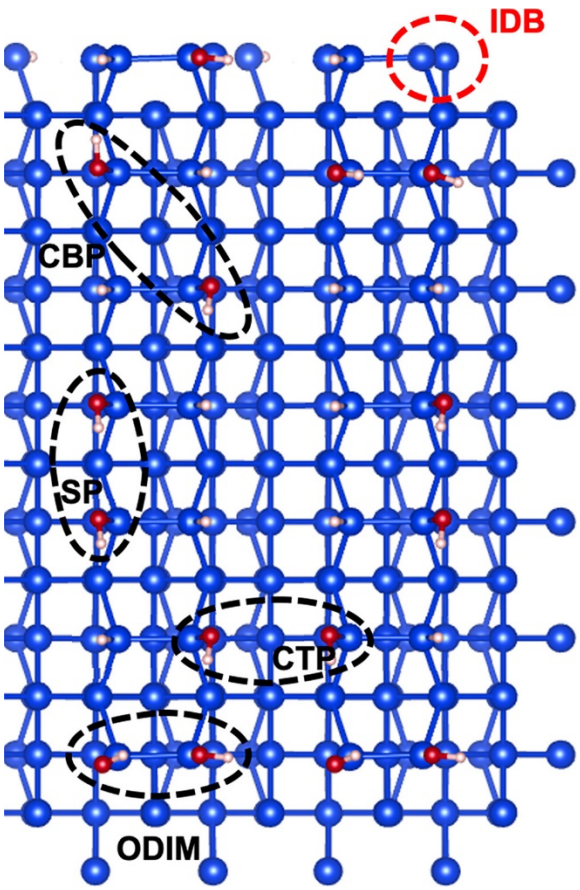

Figure 1. Ball and stick view of (H,OH)-Si(001). Silicon, oxygen, and hydrogen atoms are in blue, red and white, respectively. The OHs can form checkerboard patterns (CBP) and striped patterns (SP). On dimer (ODIM) and "cross-trench pattern" (CTP) OH pairs are also shown. The passivation of the silicon dimer dangling bonds of the 2×1 is not complete and the residual amount of tri-coordinated silicon atoms, bearing an "isolated dangling bond" (IDB), is ~4×10^{-2} ML for a n^+ substrate.[3,4]

The present paper deals with the adsorption of trimethylamine (TMA) on (H,OH)-Si(001) in the 10^{-9} mbar pressure and in the 105 K – 160 K temperature interval. It aims to answer current questions on the interaction between hydroxyls and amines but, given the presence of defects on the surface (the IDBs), it will also address the question of the reactivity of these uncapped silicon

atoms. This work can be considered as an extension of our preceding work that combined X-ray photoemission spectroscopy (XPS) with density functional theory (DFT) calculations of adsorption energies and core-level binding energies to unravel the various adsorption geometries of ammonia on (H,OH)-Si(001).[7] With respect to NH_3, TMA is expected to show significant differences in the bonding with surface OHs. First, TMA, that is a tertiary amine, can only make acceptor H bonds, while ammonia makes both acceptor and donor bonds.[7] TMA has also a greater gas-phase basicity than NH_3, 918.1 kJ mol^{-1} versus 819.0 kJ mol^{-1},[21] and this should impact the "weakening" of the H–O bond of the surface hydroxyl. The adopted methodology combines real-time synchrotron XPS of core levels, which efficiently distinguishes different chemical environments, with high resolution energy electron loss spectroscopy (HREELS), from which we expect crucial information on the O–H bond strength via the hydrogen-bonding induced redshift of the stretching mode energy. To guide the interpretation of the experimental data, cluster DFT calculations were carried out to calculate the N 1s core-level ionization energies and the vibrational mode frequencies of selected adsorption geometries. XPS shows that TMA, as a minority species, bonds to the surface IDBs and eventually breaks apart. XPS and HREELS in conjunction show that TMA, as a majority species, makes hydrogen-bonds with surface hydroxyls. In addition, HREELS provides detailed information on the nature of hydrogen-bonding, which may have an impact on the weakening of the O-H(D) bond and hence on the catalytic activity of the amine.

2. Methods

2.1 DFT quantum chemistry calculations of N 1s core-ionization and vibrational energies

The calculation procedure, making use of the GAMESS (US)[22] software, is the same as that described in detail in previous studies.[23,24,25,26] We used a "single bare dimer cluster" (Si_9H_{12}) mimicking the clean surface. To mimic the (H,OH)-surface we used clusters of various sizes depending on the TMA adsorption geometry: an "H/OH decorated single dimer cluster" (Si_9H_{12} (OH,H)), a "two-dimer-in-a-row" cluster featuring two adjacent hydroxyls sitting on two Si atoms distant by 3.84 Å ($Si_{15}H_{16}$ (2H,2OH), "striped pattern"), and a "three-dimer-in-a-row" cluster representing two non-adjacent silicon dangling bonds of the (H,OH)-Si(001) surface distant by 2×3.84 Å ($Si_{21}H_{20}$ (1H,3OH)).

Adsorption geometries of TMA used to calculate N 1s ionization energies are shown in Figure 2: (a) TMA bonded datively to a dangling bond of the water-reacted surface, with a second, non-adjacent dangling bond left free, (b) TMA dissociated via a N-C bond cleavage on the bare dimer, (c) TMA making a single acceptor hydrogen-bond (the so-called TMA(A) configuration), and finally (d) TMA making a double acceptor hydrogen-bond (the so-called TMA(A,A) configuration) with a pair of adjacent OH in a "striped pattern".

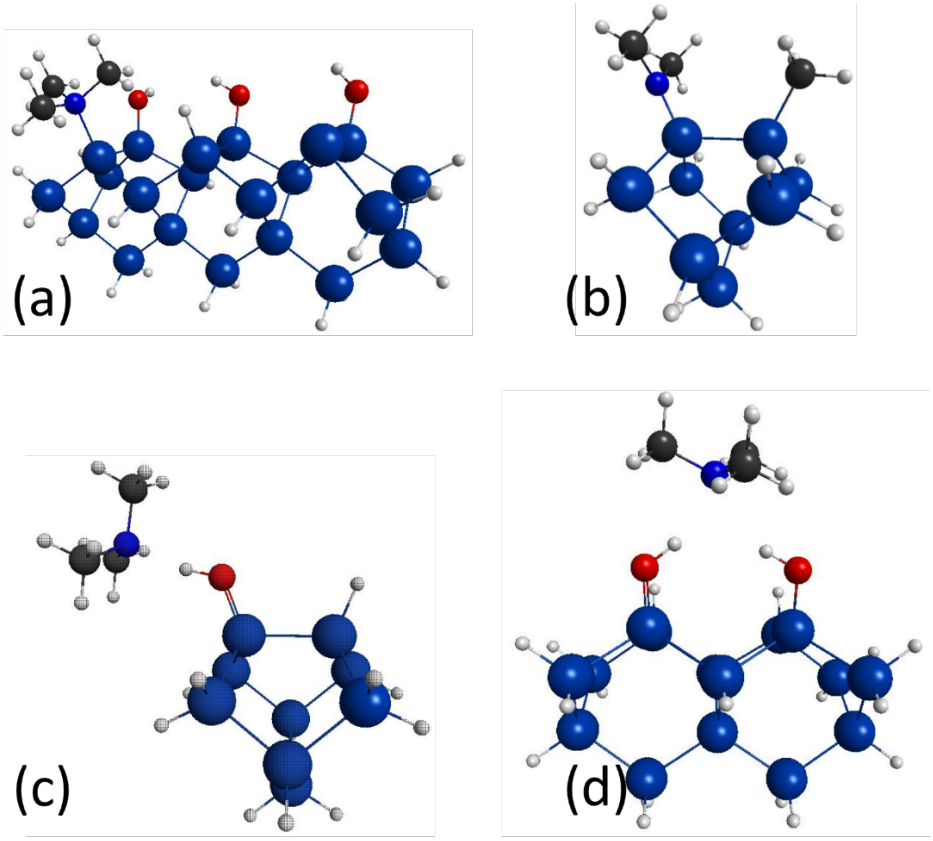

Figure 2. DFT optimized geometries: (a) TMA bonded datively to a dangling bond of a H/OH decorated three-dimer cluster, with a non-adjacent dangling bond left free, (b) TMA dissociated over a bare dimer (single-dimer cluster), (c) TMA making a single acceptor hydrogen-bond (TMA(A)) with the hydroxyl of the H/OH decorated single-dimer cluster (the N…H hydrogen-bond length is 1.755 Å), (d) TMA making a double acceptor hydrogen-bond (TMA(A,A)) with two adjacent hydroxyls of the (2H,2OH)-decorated double-dimer cluster mimicking a "striped pattern" (the N…H hydrogen-bond on the left is 2.022 Å and that on the right is 2.378 Å). Red, blue, black, and white small balls represent O, N, C and H atoms, respectively. Blue big balls are Si atoms.

Ground-state optimized geometries have been calculated using the Becke3 Lee-Yang-Parr (B3LYP) functional and effective core potentials (SBKJ + d polarization) for the substrate silicon atoms, using a 6-311G+* basis sets for carbon, nitrogen and oxygen including polarization (*) and diffuse functions (+), and 6-31G* for hydrogen. Theoretical N 1s ionization energies (IE_{QC}^{th}) were calculated as the energy difference between the core-ionized and the ground state within the ΔKohn-Sham approach and where the 6-311G+* basis set is substituted by the IGLOO III basis set on the core-hole site. Relativistic corrections (0.3 eV for N 1s) are included in the calculation. The N 1s IE_{QC}^{th}value of the isolated TMA molecule (404.7 eV) is found within 0.1 eV of the measured one (404.8 eV[27]). The "local work function"[7] Φ^{loc} is defined as:

$$\Phi^{\mathrm{loc}} = \mathrm{IE}_{\mathrm{QC}}^{\mathrm{th}} - \text{experimental binding energy (referenced to the Fermi level)}$$

As discussed in our preceding paper,[7] the IE_{QC}^{th} values of various geometries, and the calculated differences ΔIE_{QC}^{th} can only be compared to experimental binding energy shifts when Φ^{loc} (which depends ultimately on the outer electrostatic potential close to the surface) is a constant. We use here Φ^{loc}=4.45 eV, which is very close to the experimental work function of the pristine (H,OH)-Si(001) surface, 4.40 eV.[4]

The GAMESS (US) package is also used to calculate the vibrational spectra of the surface species, hydrides, hydroxyls and the probed molecule, and of the silicon atoms. The energies were determined from the Hessian matrix. The hydrogen atoms terminating the Si clusters were held in fixed positions during the frequency calculation. The spectra calculated in the dipolar approximation are plotted in the SI, section S1, Figures S1 and S2. The contributions of the three directions of space are added. All DFT vibrational energies given in the following are *rescaled* by

a factor of 0.954, obtained by comparing DFT calculated values with experimental HREELS ones (see SI, section S1, Figure S3).

2.2 Sample preparation

Preparation of (H,OH)-Si(001). The preparation of (H,OH)-Si(001) was described in detail in our preceding publications.[5,6,23] It was carried out in two separate chambers, the HREELS chamber at Bochum university, and the XPS chamber at BACH beamline (ELETTRA, Trieste).

For the XPS measurements we used a heavily phosphorus doped silicon wafer (n^+) of resistivity 0.003 Ω×cm. The clean Si(001)-2×1 surface was exposed to H_2O at 300 K for 15 min under a nominal pressure of 4.5×10^{-9} mbar, which is certainly underestimated because the gauge is far from the sample (see below, exposure to TMA). Thus, the water dose Q_{water} (number of water molecules having hit the surface per surface unit) expressed in silicon monolayers[4] (1 ML =6.8 10^{14} molecules/cm^2) was at least equal to 2.25 ML. Under 4.5×10^{-9} mbar of water, the surface is saturated for $Q_{water}\geq$ 1 ML.[4]

For the HREELS experiments we used lightly *n*-doped Si(100) wafers of resistivity ~1000 Ω×cm to avoid plasmon excitations which result in a broadening of the quasi-elastic peak.[28,29] The clean Si(001)-2×1 surface was exposed at 300 K to a water dose Q_{water} equal to 1.5 ML, either H_2O or D_2O (isotopic enrichment 99.98%). The careful preparation of the (D,OD)-Si(001) surface resulted in a D to H ratio of 16:1 at saturation coverage determined from the HREELS peak area ratio of the Si-H↕ and Si-D↕ stretching modes (↕ means perpendicular to the surface, "out of plane"). The excess of ^{1}H species with respect to the nominal isotopic ratio is likely due to H_2O

molecules adsorbed on the chamber walls and displaced during the exposure to D_2O. The DFT vibration energies (rescaled values) of the TMA(A) model configuration (see SI, section S1, Figure S1(a)) place the unperturbed SiO-H ↔ mode (↔ means parallel to the surface, "in plane") at 460 meV and the red shifted SiO-H↔TMA modes due to hydrogen-bonding at 351 and 372 meV, mixed with methyl vibration modes. For its part, the SiO-D ↔ mode of the isolated hydroxyl is calculated at 335 meV (see SI, section S1 Figure S2(a)), and the SiO-D ↔ TMA mode at 271 meV (ΔE=64 meV), well separated from the methyl modes at 353-369 meV (see Figure S2(b)). Therefore, D_2O is used instead of H_2O to measure the red shift of the SiO-D ↔ stretching energy of OD in interaction with TMA. However, to follow the hydroxyl-TMA interaction with increasing TMA dose, it can be more convenient to follow the damping of the SiO-H ↔ mode of the unreacted SiOH, calculated at 460 meV, than that of the SiO-D ↔ mode of the unreacted SiOD at 335 meV, which is too close to the methyl modes (353-369 meV).

Exposure to TMA during XPS measurements. During real-time XPS measurements, the (H,OH)-Si(001) surface is exposed to TMA at 130 K. The nominal pressure measured by the hot cathode ionization gauge is 1.1×10^{-9} mbar (considering the relative sensitivity factor R_g of 4.7 for TMA[30]). However, this nominal pressure gives an unphysical sticking coefficient greater than one because the real pressure at the sample is underestimated (the gauge is far away from the sample). To get ~0.12 ML of TMA adsorbed in 140 s (see below) with a sticking probability of one, we must consider a corrected TMA pressure p_{TMA}^{corr} of ~3×10^{-9} mbar. TMA doses (Q_{TMA}, also expressed in Si ML) are calculated with p_{TMA}^{corr}.

Exposure to TMA in the HREELS chamber. The adsorption behavior of TMA is investigated under 1×10^{-8} mbar (the pressure is corrected by the sensitivity factor R_g), in the temperature range between 105 K and 160 K. TMA desorption is found at T>175K.

2.3. XPS at ELETTRA Synchrotron Facility (Trieste)

Electron spectroscopy measurements were performed at BACH Beamline, ELETTRA synchrotron facility (Trieste, Italy). Linearly polarized light in the 175-600 eV range is provided by a high energy APPLE II helical undulator. The photon dispersion system is based on a PADMORE variable angle spherical grating monochromator. Photoemission spectra were measured by means of a modified 150 mm VSW hemispherical electron analyzer with a 16-channel detector. In the adopted geometry, the photon beam direction was perpendicular to the sample surface (the polarization was contained in the surface plane) and the photoelectron emission angle was at 60° from the sample surface. The N 1s and O 1s spectra were measured at 455 eV and 595 eV, respectively. The Si 2p core level spectrum of the (H,OH)-Si(001) surface were measured at hν=175 eV and 350 eV. The spectra, after Shirley background subtraction, are fitted with sums of Gaussians. Only the N 1s spectra are shown in the main paper. The nitrogen surface density was obtained by measuring the area under the N 1s peak and comparing it to the N 1s spectral area of the (H,NH_2)-Si(001) surface, that corresponds exactly to 0.5 ML.[25] The Si 2p and O 1s spectra are presented and discussed in the SI, section S2. After exposure to water at room temperature, the Si 2p spectrum (Figure S4, section S2 of the SI) is characteristic of the surface saturated by water fragments. The "up dimer atom" component is quenched and a SiOH component shows up. After cooling down to 130 K, a control Si 2p spectrum (section S2 of the SI Figure S5) shows that the spectral shape is not changed (therefore there is no further oxidation due to possible residual molecular water condensation on the surface). The O 1s spectrum measured at

300 K (section S2 of the SI Figure S6) is fitted with a main single narrow component at the characteristic BE of OHs and a minor component (9 % of the spectral weight) due to siloxane bridges.[23] Together with the low spectral weight of the Si^{2+} oxidation state in the Si 2p spectrum, this shows that subsurface oxidation is minor, and hence that the starting cleaned surface was smooth.

The few IDBs remaining on the surface (~$4.0\pm0.4\times10^{-2}$ ML) are doubly occupied and hence negatively charged.[4] They cannot be directly detected as a component in the Si 2p core levels, but they fix the position of the Fermi level at the surface, and hence the Si 2p binding energy, 99.41 eV at 300 K.[4] However, after cooling down the substrate, the Si 2p spectrum moves slightly to higher binding energy, because of a surface photovoltage (SPV) effect that decreases the upward band bending[4] at the surface (the sample in n^+-doped). Due to the SPV, the binding energies of the N 1s and C 1s spectra acquired at low temperature and shown in the following are corrected, keeping the Si $2p_{3/2}$ binding energy at 99.41 eV (its position at room temperature) just after water dosing.

2.4 HREELS at Bochum University

The HREELS-experiments were performed at Bochum University in a separate chamber equipped with a toroid-spectrometer (Gossmann electron optics, design H. Froitzheim) capable of achieving an energy resolution of 1 meV. In the present experimental conditions, a resolution of the spectrometer of 3.5 meV was used, resulting in a full width at half maximum (FWHM) of the elastically reflected peak of 7-10 meV. All vibrational spectra shown here are taken in the specular configuration ($\theta_I = \theta_f = 60°$ with respect to the surface normal) with a primary beam energy E_p of 5 eV. The HREELS spectra are corrected by subtracting an exponential background[31] as well a

constant background arising from prominent overtone/multiple loss features between 100-360 meV.[32] Normalization to the elastic peak intensity (as commonly used to improve the comparability between HREELS spectra independent of absolute electron count-rates) did not yield suitable results due to an overall reduced dipole scattering character of all internal molecule modes of TMA adsorbed on pristine Si(100) and the water-covered surface. This is experimentally identified by a weak angular dependence of the corresponding loss peak area versus off-specular angle. Especially in the TMA-(H,OH)-Si(100) system the ν(CH_3) and in-plane (↔) ν(SiO-H)/ν(SiO-D) peak area show hardly any change with increasing off-specular angle, which indicates excitation via impact- or resonant- rather than dipole-scattering.[33] In contrast, the out-of-plane (↕) Si-H/Si-D and Si-OH/Si-OH stretching modes obey the dipolar selection rule and require a usual normalization to the elastic peak intensity. As our discussion of HREELS is based on characteristic changes in the energy loss regime above 200 meV, where the loss mechanism is dominated by impact scattering, all shown spectra are only normalized to the elastic peak intensity of the initial spectrum (taken as a reference) of a given set of consecutive spectra.

3. Results and Discussion

3.1 Real-time XPS at 130 K

The first step of the real-time XPS experiment consisted in exposing the (H,OH)-Si(001)-2×1 to TMA, for 140 s, at 130 K and under p_{TMA}^{corr} = 3×10^{-9} mbar (Q_{TMA}=0.12ML), after which the leak valve was closed, and TMA was pumped down.

During the exposure and subsequent pumping, the N 1s spectra were continuously recorded in swept mode (it takes 30 s to acquire one spectrum). Illustrative spectra are shown in Figure 3(a). Immediately after dosing, the spectrum exhibits two components at experimental binding energies of ~402.4 eV and ~400.5 eV, respectively. Then, while the chamber is pumped down, a new peak appears at lower BE, at ~399.3 eV. Fifty-one spectra from the real-time experiment are fitted with the three components shown in Figure 3(a). In Figure 3(b), we plot against time the total nitrogen coverage (expressed in ML), as well as those of the various chemical components.

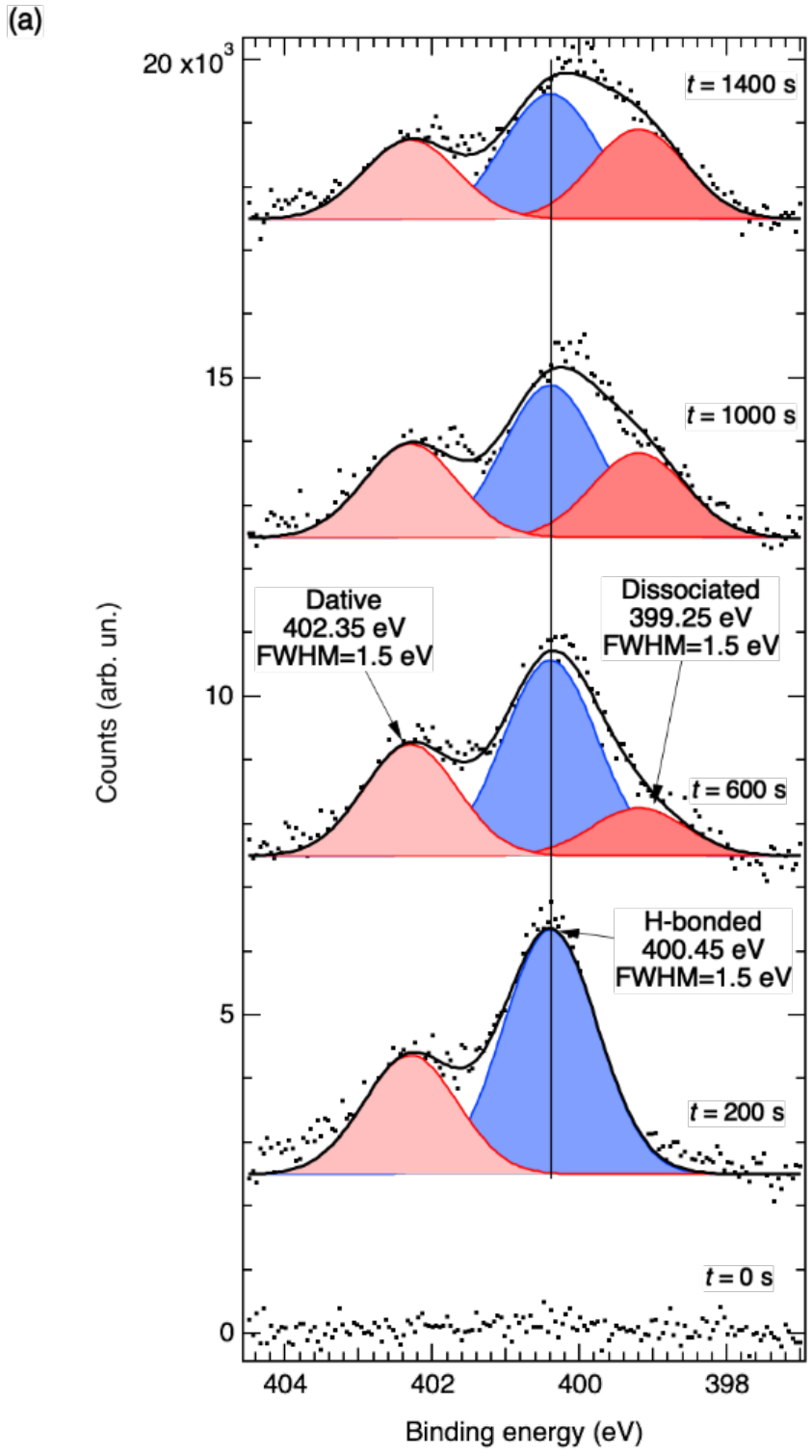
(a)
20 x10^3
15
10
5
0
t = 1400 s
t = 1000 s
Dative
402.35 eV
FWHM=1.5 eV
Dissociated
399.25 eV
FWHM=1.5 eV
t = 600 s
H-bonded
400.45 eV
FWHM=1.5 eV
t = 200 s
t = 0 s
Counts (arb. un.)
404
402
400
398
Binding energy (eV)

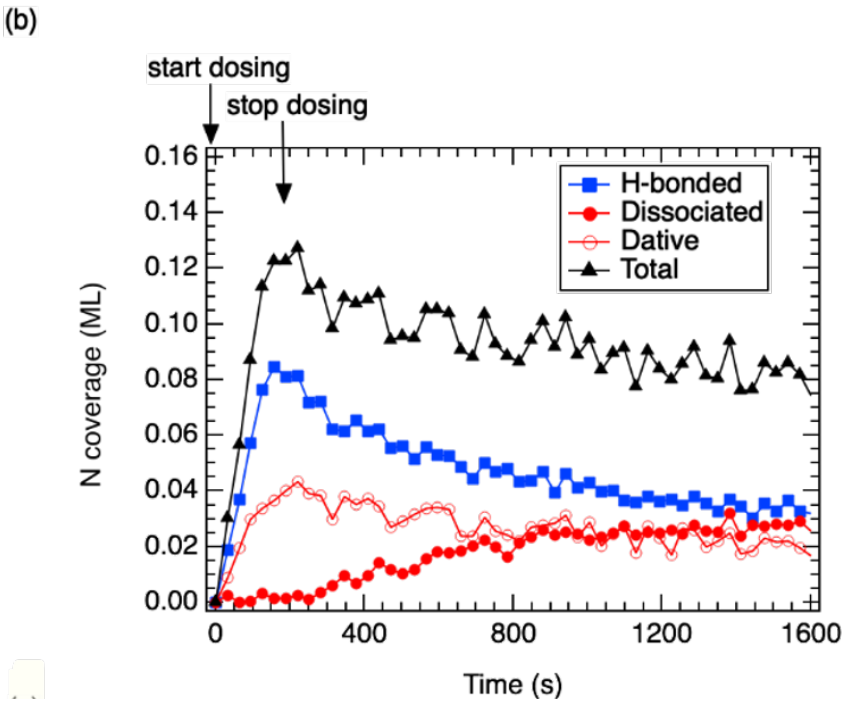

Figure 3. (a) Illustrative N 1s spectra measured at 130 K with a photon energy hν of 455 eV. TMA dosing (under 3×10^{-9} mbar) is interrupted after 140 s, then the analysis chamber is pumped down. Each shown spectrum is integrated over a time interval of 200 s. The curves are fitted by sums of Gaussians whose FWHM and binding energies (referenced to a common Si $2p_{3/2}$ binding energy at 99.41 eV) are indicated. (b) Real-time kinetics of the adsorbed species (surface densities are expressed in ML) distinguished by their binding energies (dissociated, hydrogen-bonded and datively bonded).

We start discussing the minority species found at an experimental binding energy of ~402.4 eV. After 140 s of dosing, the coverage of this species is 0.04 ML (Figure 3(b)). This coverage is comparable to the IDB surface density determined by STM, ~0.04 ML.[3] We consider that TMA molecules can bind to these uncapped silicon atoms via a dative bond. Indeed, the BE of ~402.4

eV matches exactly that of tertiary amines (TMA[34] and triethylamine[35]) datively bonded on *clean* Si(001)-2×1. Indeed, we made the same observation when the (H,OH)-Si(001) surface was exposed to ammonia at 130 K, as we found a minority species (maximum coverage~0.04 ML) at a high BE of 401.7 eV, attributed to the dative bonding of NH_3 with an IDB.[7] The adsorption geometry depicted in Figure 2(a) shows that the dangling bonds are not necessarily adjacent (as it is the case for the clean surface). Figure 2(a) shows also interesting features that are a manifestation of the local charge density. One can note that the H atom of the hydroxyl facing the adsorbed molecule is repelled. This indicates that the molecule is electron-poor (the Lewis structure is Si-$N^{\oplus}(CH_3)_3$, the datively bonded nitrogen bearing a positive formal charge). On the contrary, the hydrogen of the hydroxyl placed in front of the unoccupied silicon dangling bond is attracted to the latter. This shows that the remaining dangling bond is electron-rich (indeed the dimer buckles, with the "negative" silicon moving up). This calculation simply suggests that dative bonding on an IDB is feasible only when an electron "sink" is available. On the real, extended surface, the electronic charge could be pushed away from the surface into bulk silicon by the insertion of the Lewis base lone pair into the IDB. In fact, for an n^+ substrate, the dangling bond is indeed doubly occupied, i.e. negatively charged.[3,4] Therefore, one would expect TMA to be repelled when it approaches the tri-coordinated silicon adsorption site. As a dative bonding is observed, this means that the electron charge on the silicon defect is delocalized into the substrate. We recall that the adsorption of ammonia molecules and amines on *n*-type H-terminated Si(111) (via bonding with surface IDBs) induces a strong electron-accumulation layer close to the surface.[36] Unfortunately band bending changes cannot be detected by Si 2p binding energy changes[4] because of SPV at low temperature.

The other minority species has a binding energy of ~399.3 eV. This binding energy matches with that of the dimethylamino Si-N$(CH_3)_2$ moiety of TMA dissociated on the bare dimer of the clean surface via N-C bond cleavage[34] (see Figure 2(b)). It can also correspond to a methylamino unit Si-$NHCH_3$ whose presence suggested by the analysis of the C 1s spectra (see below). The kinetics in Figure 3(b) show that the increase in coverage of dissociated TMA (0.02 ML at 1600 s) correlates with the decrease of the datively bonded species, suggesting that the latter species is the precursor of the former one.

The experimental binding energy (referenced to the Fermi level) of minority species constitutes a benchmark of the theoretical N 1s ionization energies (referenced to the vacuum level). This leads to an effective work function Φ^{loc} of 4.45 eV that enables the calculation of the theoretical binding energies ($IE_{QC}^{th} - \Phi^{loc}$) that are compared in Table 1 to the experimental ones.

Species	Cluster type	IE_{QC}^{th} (eV)	$IE_{QC}^{th} - \Phi^{loc}$ (eV)	Measured binding energy (eV)
Isolated $N(CH_3)_3$	-	404.7*	-	-
Trimethyl-ammonium $N(CH_3)_3H^+$	-	414.4	-	-
Dissociated TMA bare dimer	Si_9H_{12} $(CH_3,N(CH_3)_2)$	403.7	399.25	399.25
hydrogen-bonded TMA(A)	Si_9H_{12} $(H,OH,N(CH_3)_3)$	405.3	400.85	400.45
hydrogen-bonded TMA(A,A) (striped pattern)	$Si_{15}H_{21}$ $(2H,2OH,N(CH_3)_3)$	405.4	400.95	400.55
Dative bonding $Si\text{-}N^{\oplus}(CH_3)_3$	$Si_{21}H_{20}$ $(1H,3OH,N(CH_3)_3)$	406.8	402.35	402.35

Table 1. Calculated values of N 1s ionization energies (IE_{QC}^{th}) for gas phase TMA (the experimental value is 404.8 eV[27]), trimethylammonium, and the TMA adsorption geometries considered in Figure 2. Calculated N 1s binding energies ($IE_{QC}^{th} - \Phi^{loc}$) referenced to the Fermi level using a local work function Φ^{loc} of 4.45 eV. Experimental N 1s binding energies (referenced to Si $2p_{3/2}$ at 99.41 eV) that best correspond to the cluster model values.

Now we focus on the majority species at ~400.5 eV. The kinetics in Figure 3(b) shows that at 140 s (Q_{TMA} =0.12 ML), the coverage reached by this species is 0.08 ML. When the TMA pressure goes to zero after stopping the dosing, the coverage decreases by 0.04 ML between 140 s and 1600

s. The total nitrogen coverage (Figure 3(c)) also diminishes by the same value during the same duration, which shows that this desorbing species is more weakly bound to the surface than TMA datively bonded to the IDB or the Si-NC_x moiety. The observed desorption suggests that the main component in the N 1s spectrum is likely related to hydrogen-bonded TMA molecules. In the N 1s DFT calculations, we have both considered the single-acceptor TMA(A) and the double-acceptor TMA(A,A) configurations. Indeed, the maximum coverage reached during the real-time XPS experiment (0.08 ML) is significantly less than the OH one (0.5 ML). Thus a TMA molecule can not only interact with a single OH (the TMA(A) configuration in Figure 2(c)) but also with pairs of adjacent OHs, for instance on a striped pattern (SP) of Figure 1 (mimicked by the TMA(A,A) configuration of Figure 2(d)). Interaction with OH pairs sitting on the same dimer (the ODIM site of Figure 1) could also be envisioned, but such a configuration being a minority one, see ref[3], we have skipped its study. We find that IE_{QC}^{th} (see Table 1) is 405.3 eV for TMA(A) and 405.4 eV for TMA(A,A). Therefore, the two configurations cannot be distinguished by XPS (in contrast the differences in the HREELS vibrational spectra are much more dramatic, see section 3.2). Thus, the expected binding energy (measured from the Fermi level) is *ca* 400.9 eV for both configurations. This value is only ~0.4 greater than the measured binding energy of the main peak (~400.5 eV). This lends support to the attribution of the main component to hydrogen-bonded TMA. Hints of the formation of hydrogen-bonds between surface OHs and TMA are difficult to extract from the O 1s spectra (see SI, Figure S6). With respect to the spectrum of the pristine surface at 300 K, the O 1s peak broadens at low temperature in the presence of TMA (the FWHM increases by 0.5 eV), but this can be due to hydrogen-bonding both between surface OHs and between OHs and TMA molecules. The N 1s spectra also show that the proton transfer from a hydroxyl to TMA is completely excluded in the present UHV conditions. The free

trimethylammonium ion has a very large IE_{QC}^{th} of 414.4 eV. If the $N(CH_3)_3H^+$ ion were sitting on the surface, it should exhibit a binding energy of ~410 eV, considering Φ^{loc}, which is not observed.

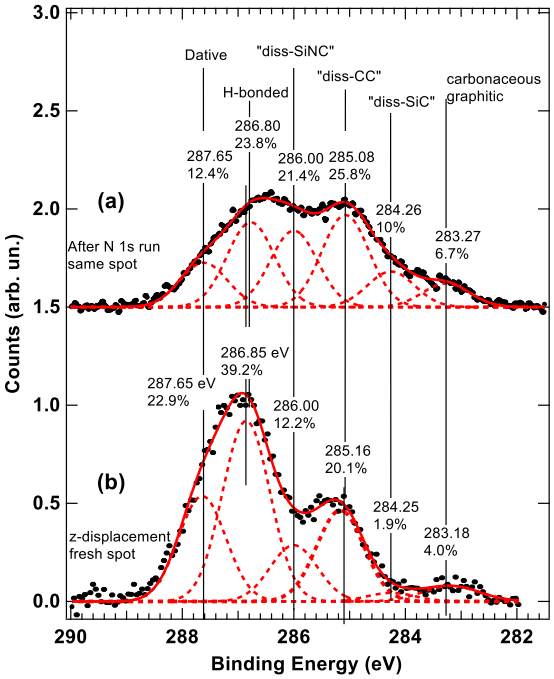
Dative
"diss-SiNC"
"diss-CC"
"diss-SiC"
carbonaceous
graphitic
H-bonded
286.80
23.8%
287.65
12.4%
286.00
21.4%
285.08
25.8%
284.26
10%
283.27
6.7%
(a)
After N 1s run
same spot
286.85 eV
39.2%
287.65 eV
22.9%
286.00
12.2%
285.16
20.1%
284.25
1.9%
283.18
4.0%
(b)
z-displacement
fresh spot
Counts (arb. un.)
Binding Energy (eV)
3.0
2.5
2.0
1.5
1.0
0.5
0.0
290
288
286
284
282

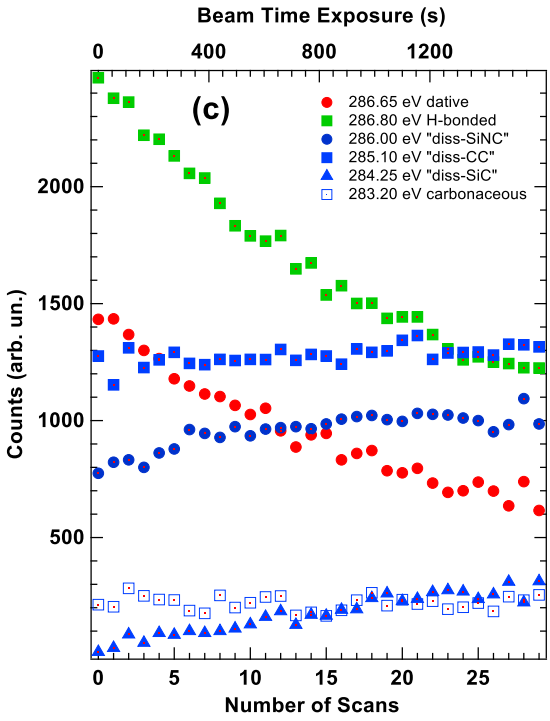

Figure 4. Control C 1s spectra (hν=350 eV). Curve (a) measured immediately after the real-time N 1s XPS monitoring on the same spot (~2000 s after the 140 s TMA dosing and continuous irradiation). Curve (b) measurement on a "fresh spot" (~2000 s after the 140 s TMA dosing, no

previous irradiation) after a vertical displacement of the sample holder. The curves are fitted by sums of Gaussians of FWHM equal to 1.0 eV. Binding energies (referenced to a common Si $2p_{3/2}$ binding energy at 99.41 eV) and spectral weights are indicated. Curve (c) shows the effect of time and beam exposure starting from a "fresh spot" (scan#0) as in curve (b).

We also checked the consistency of the decomposition of the C 1s spectrum given in Figure 4 with the interpretation of the N 1s spectrum. The C 1s spectrum (a) is recorded immediately after the end of the real-time N 1s XPS experiment, keeping the same measurement position, while spectrum (b) is measured at a position untouched by the X-ray beam ("fresh spot"). The curves in Figure 4(a,b) are normalized to equal acquisition times. Figure 4(c) shows the evolution of the various component intensities with time, starting from a "fresh spot" (curve (b)). To obtain consistent binding energies in fitting curves (a) and (b), we had to use six peaks of equal FWHM (1.0 eV). The fitting of curves (a) and (b) shown in the SI, section S2, Figure S7 with less (four) but broader Gaussians (FWHM=1.2-1.3 eV) gives inconsistent binding energy. In particular the presence of components at ~286.0 eV and ~284.3 eV was proven particularly indispensable.

The peak at ~287.65 eV corresponds to the datively-bonded species.[34] The structure at 286.85 eV is attributed to the hydrogen-bonded molecule. It could also be a Si-O-CH_3 component (~286.7 eV[37]), resulting from a reaction of TMA with a hydroxyl. However, as it tends to decrease with time/beam exposure (see Figure 4(c)), this hypothesis is rejected. The component at 286.00 eV has the same binding energy as that of C atoms first neighbors to N atoms in alkylamino units, (the core ionized carbon is denoted $\underline{C}$), like Si-N($\underline{C}H_3)_2$ and Si-NH-$\underline{C}H_2$-CH_2-CH_2-$\underline{C}H_2$-NH-Si of TMA and diaminobutane, respectively, when they are dissociatively adsorbed on clean S(001).[38,39] This

component will be denoted “diss-SiNC” in the following. The well-marked peak at 285.1 eV coincides with the binding energy of C atoms, second neighbor to N ones, as in Si-NH-CH_2-$\underline{C}H_2$-$\underline{C}H_2$-CH_2-NH-Si.[39] It also matches the C 1s of hydrocarbon polymers (285.0±0.2 eV).[40] Note that a light hydrocarbon like C_2H_6 does not stick on the clean S(001) surface at 90 K,[41] and thus the hydrocarbons should attain a sufficient molecular weight to be present at 130 K. The peak at 285.1 eV will be denoted “diss-CC”. It cannot be mistaken with the Si-$\underline{C}H_3$ component (denoted “diss-SiC”) which is ~0.8 eV lower in energy at ~284.3 eV.[35,37,42] The peak at ~283.2 eV is generally attributed to carbonaceous/graphitic compounds,[43] and it remains constant with time in Figure 4(c).

The comparison of curves (a) and (b) is helpful to determine the beam damage effects. On a fresh spot, both the datively- and hydrogen-bonded species components are more intense than on the heavily-irradiated spot, which indicates that the beam tends to facilitate the decomposition of the former and the desorption of the latter. In fact, the “dative” (287.7 eV) to “diss-SiNC” (286.0 eV)” intensity ratio is 1.9 on the “fresh spot”, but only 0.58 on the “heavily-irradiated” spot, which indicates that X-rays accelerate the dissociation of Si-$N^{\oplus}(CH_3)_3$. We made exactly the same observations for NH_3 datively bonded to the IDBs of (H,OH)-Si(001).[7] In Figure 4(c) (where scan #0 is a “fresh spot” spectrum), we indeed observe the decrease of the H-bonded species and of the dative “component” with time/irradiation and the increase of the Si-NC^1 intensity. It is remarkable that in the “fresh spot” spectrum (Figure 4(b)), we see the “diss-SiNC” unit and the “diss-CC” peaks, but the intensity of the “diss-SiC” component is practically zero. The latter only appears after prolonged irradiation (Figure 4(a)). These trends are also shown by the kinetics of Figure 4(c), where the “diss-SiC” peak intensity increases of with time from ~0 (scan#0). This suggests

that there are two decomposition channels, one in the dark leading to "diss-SiNC" and "diss-CC" products, and the other, specific to X-ray irradiation that leads to "diss-SiNC" and "diss-SiC".

To better understand the mechanisms at work, we examine now the carbon ratios of the dissociation products. The intensity ratio between the components "diss-CC" at 285.1 eV and that of the "diss-SiNC" at 286.0 eV is ~1.7 (see Figure 4(b) and the peak intensities of scan #0 in Figure 4(c)).

If one assumes a reaction in which only *one* N-C bond of the dative species ($Si\text{-}N^{\oplus}(CH_3)_3$) breaks to form one dimethylamino $Si\text{-}N(CH_3)_2$ adduct leaving one CH_3 that further reacts with other CH_3 to form a hydrocarbon, or a more complex reaction in which the end product contains one carbon that is 2nd neighbor to the nitrogen atom (like in $Si\text{-}N(CH_3)(CH_2\underline{C}H_3)$), then the "diss-CC" to "diss-SiNC" intensity ratio will be 0.5, which is not observed.

Therefore, we need to consider a reaction in which *two* N-C bonds of the dative species are broken, to form an alkylamino species with only *one* C first neighbor to N. This unit would be necessarily Si-NHC-. The H atom can be provided by a SiH adjacent to the IDB where the datively-bonded species is adsorbed. Indeed H jumps on a π-molecule sitting on a silicon dangling bond are well-documented in the case of H-terminated surfaces.[44–46] The final products could be a $Si\text{-}NH(CH_3)$ ("diss-SiNC") and hydrocarbons ("diss-CC") resulting from the recombination of the leaving methyls. Alternately, a complex reaction would lead to a product where the two leaving carbons are attached to the alkylamino unit as 2nd or 3rd neighbors to the nitrogen. In a structure like $Si\text{-}NHCH_2\underline{C}H_2\underline{C}H_3$ unit the underscored atoms will be of the "diss-CC" type with a binding energy of 285.2 eV. In any case, when two N-C bonds are broken, the "diss-CC" to "diss-SiNC" intensity ratio will be 2, a value much closer to what we measure (1.7).

Once the X-ray beam irradiates the "fresh spot", see Figure 4(c), the intensity of the "diss-SiC" component at ~284.3 eV starts to increase from zero, together with that of the "diss-SiNC" component at 286.0 eV. In the meanwhile, the intensity of the "diss-CC" peak at 285.2 eV remains rather constant, hence "diss-SiC" does not grow at its expenses. Therefore under the beam the favored reaction could involve one N-C bond break, to give a Si-N$(CH_3)_2$ and a Si-CH_3, as it is the case for the clean surface. X-ray beam irradiation could facilitate N-C bond breaking in the datively-bonded molecule through an attachment-dissociation reaction involving secondary electrons.[47] The liberated CH_3 radical could react locally by breaking a Si-Si bond or diffuse farther away until it finds an IDB distant, at an average distance of 2-3 nm, given the IDB coverage of a few hundredths of ML. Such a long distance mechanism is suggested for water adsorbates on (H,OH)-Si(001).[11]

3.2 HREELS in the 105 K-160 K temperature interval

We show in Figure 5 the HREELS spectra of (H,OH)-Si(001) at 120 K and (D,OD)-Si(001) at 160 K before and after exposure to TMA in the upper and lower panel, respectively. The HREELS spectra of clean dimerized Si(001) at 300 K before (a) and after TMA dosing (a') are given for the sake of comparison. The energy loss assignments are also given.

The HREELS spectra of (H,OH)-Si(100) (curves 5(b) and 5(b')) and (D,OD)-Si(001) (curves 5(c) and 5(c')) exposed to TMA both confirm that the majority species is molecularly adsorbed. Indeed, all the characteristic internal TMA vibrational modes show up (see also the SI, section S1, Table S1, where the vibration energies of the gas and solid phase are collected). The comparison with the clean silicon surface (curves 5(a) and 5(a')) is useful, as on this surface TMA *does not*

break. We notice that the NC_3 and CH_3 groups at ~159 meV (red-shaded), ~130 meV (green-shaded) and ~369 meV (green-shaded) appearing in curves 5(b') and 5(c') are in proportions similar to those seen in curve 5(a'). Thus, HREELS shows that *most* molecules are intact on the water-covered surface.

Now, do the minority species detected by XPS appear in the HREELS spectra? For what regards the datively bonded species, there is no reason why TMA should not bond to an IDB on the lightly doped *n* substrate used in the HREELS experiments, as its electron occupancy is practically one.[4] In fact, to donate its nitrogen lone-pair, the TMA molecule would have less charge to displace than on the n^+ substrate of the XPS study for which the IDB occupancy is two.[4] The characteristic Si-N ↕ stretching mode of the datively-bonded species is predicted by DFT at 63 meV, (rescaled value, see SI, section S1, Figure S1(b)). It is indeed observed as a prominent feature (yellow-shaded) for TMA adsorbed on clean Si(001) (curve 5(a′)) at 66 meV (see also the previous works[48,49,50]). However, in the case of the water-covered surface, its observation and weighing by HREELS is difficult for two reasons: first, the datively-bonded geometry is a minority species, second, its characteristic Si-N mode overlaps with other TMA modes (e.g. the methyl mode at 54 meV) and the silicon phonon modes (at ~62 meV, see also the calculated silicon cluster frequencies in the SI, section S1). The second minority species, the dissociated molecule, can be under the form of of $Si\text{-}NHCH_3$ and aliphatic carbon, or of $Si\text{-}N(CH_3)_2$ and $Si\text{-}CH_3$ as shown by XPS. In fact, the $Si\text{-}N(CH_3)_2$ ↕ stretching mode and the $SiCH_3$ (sym) + $N(CH_3)_2$ (symmetric and antisymmetric) are expected from DFT calculations (rescaled values) at 116.4 meV and 357.7 meV, respectively. These modes appear in a very crowded region of the energy loss spectrum (see Figure 5). Distinguishing modes associated to these fragments is also practically impossible. Thus, for what

regards the detection of the present minority species XPS was more informative than HREELS.

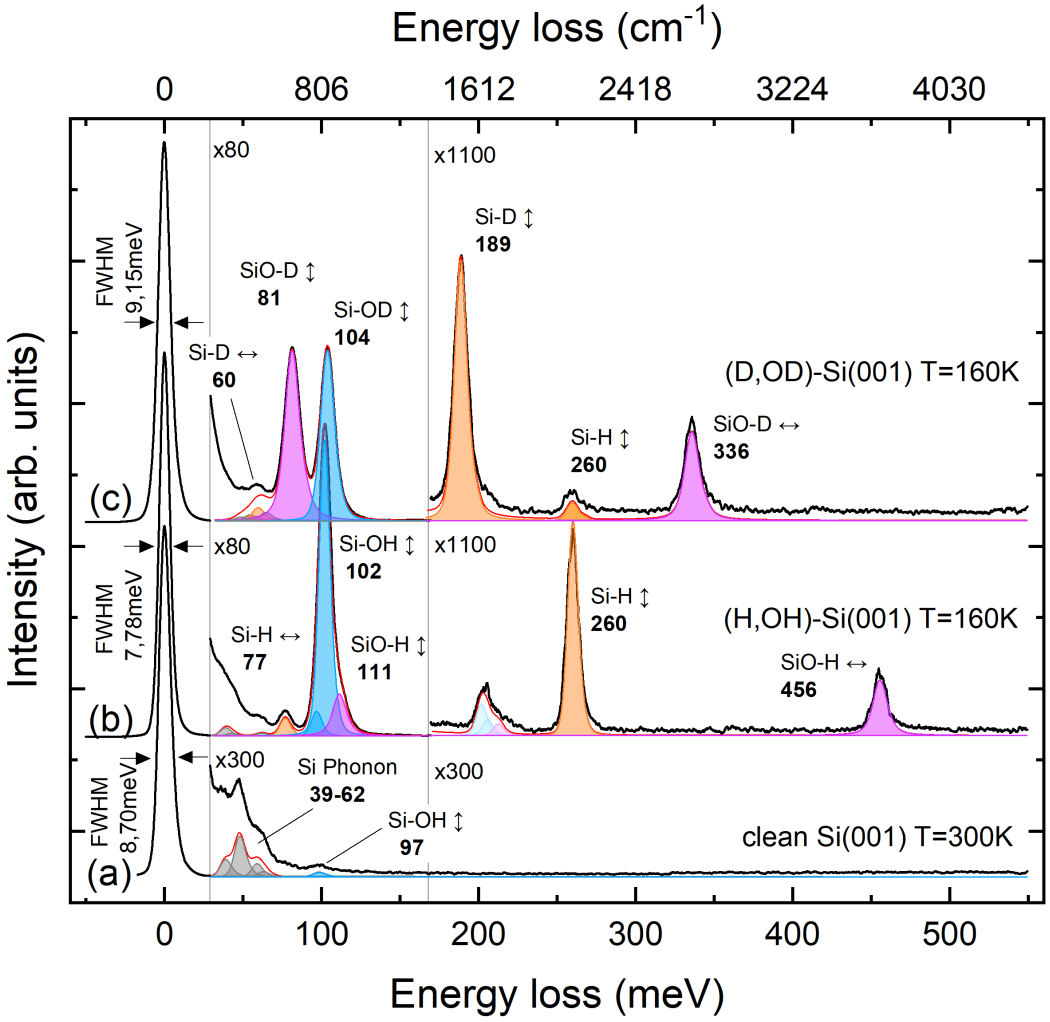

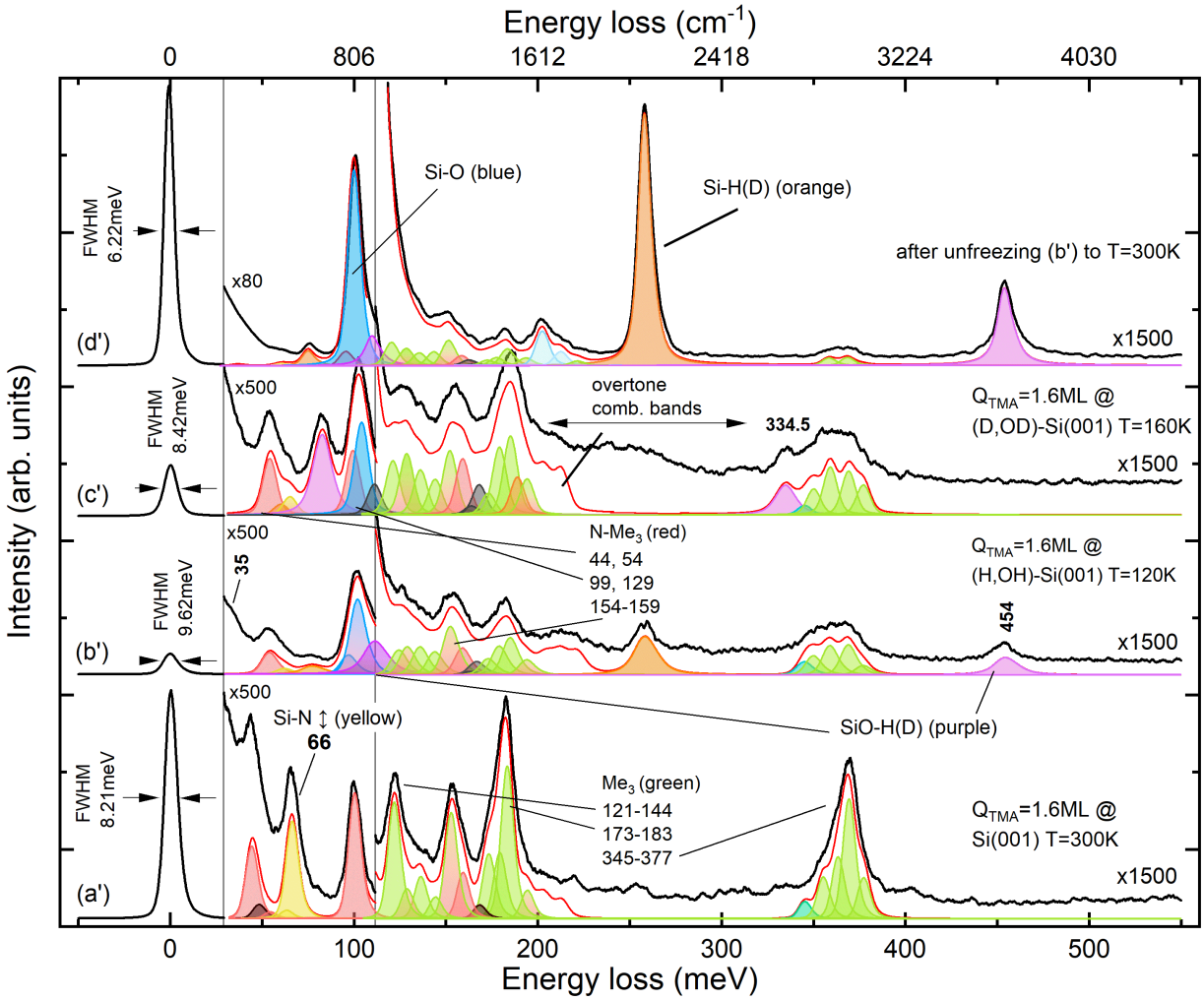

Figure 5. HREELS spectra (black curve) and peak-deconvolution after background subtraction (red line) of (a) clean Si(100)-2×1 at 300 K and (a') exposed to Q_{TMA}=1.6 ML at 300 K, (b) (H,OH)-Si(100) at 120 K and (b') exposed to Q_{TMA}=1.6 ML at 120 K, (c) (D,OD)-Si(001) at 160 K, (c') exposed to Q_{TMA}= 1.6 ML at 160K and (d') shows (b') after unfreezing to T=300 K. Peak positions in the figure are given in meV. "Me" is for CH_3. Color code: Si phonons (grey), SiO-H/SiO-D (purple), Si-H/Si-D (orange), Si-O (blue), Si-N (yellow), N-Me_3 (red), Me_3 (light/dark green) and non-attributed (black).

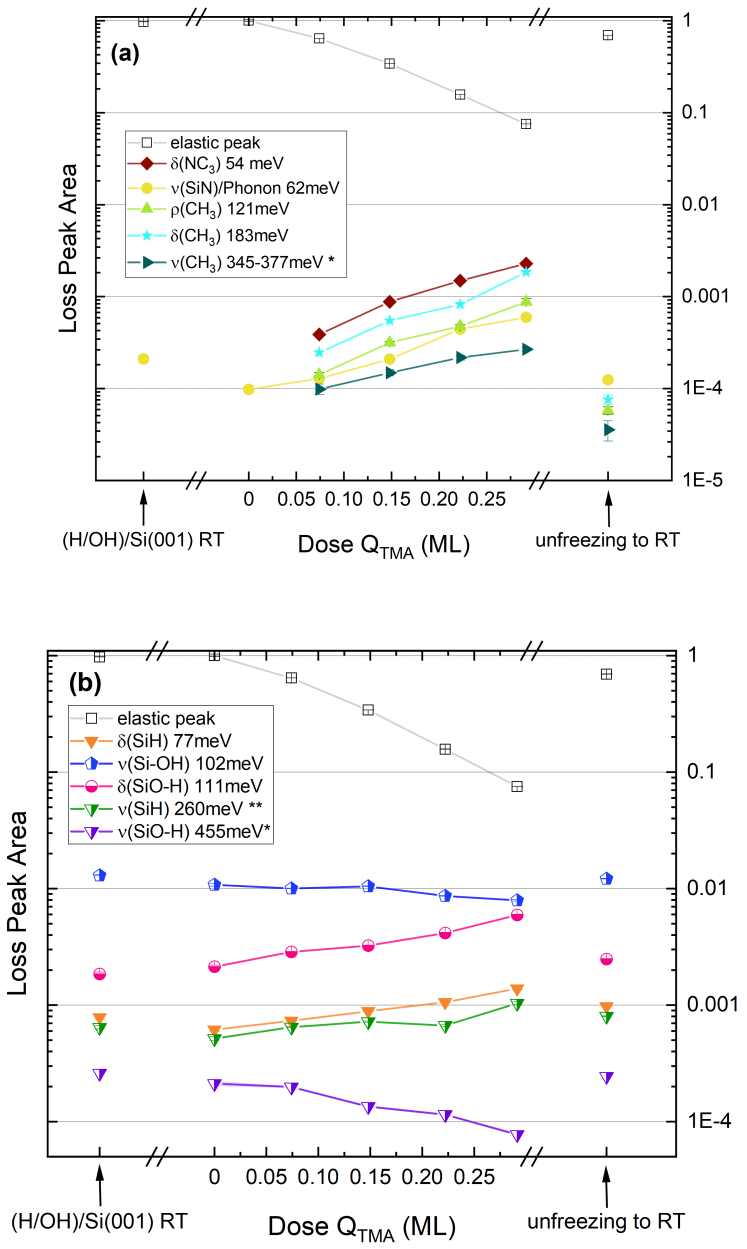

Figure 6. HREELS peak progression (logarithmic scale) of surface bound TMA mode intensities (panel (a)) and hydride/hydroxyl ones (panel (b)) with increasing TMA dose Q_{TMA} during exposure of (H,OH)-Si(001) to gaseous TMA at 120 K. Peak areas are normalized as described in the text with * indicating normalization to common reference. ** linear subtraction of TMA multiple losses/overtone background.

The monitoring of the sub-monolayer adsorption process with increasing Q_{TMA} at 120 K on (H,OH)-Si(001) is shown in Figure 6(a). The TMA vibrational loss intensities increase with increasing Q_{TMA} (at 120 K) until saturation is reached for Q_{TMA} above 0.30 ML. Figure 6(b) shows that the Si-H mode at 77 meV remains practically unaffected. Thus, TMA does not form bonds with the hydride, nor can it abstract it in amounts sufficiently large to be detectable by HREELS. A similar observation was made when water molecules adsorb on (H,OH)-Si(001).[51] In stark contrast, the O-H stretching mode is strongly perturbed by TMA adsorbed on the surface as its intensity at 455 meV decreases with increasing TMA coverage. This can be explained by the fact that the TMA molecule makes hydrogen-bonds with the surface hydroxyls. We recall that possibly red-shifted O-H modes cannot be observed as they mix with methyl modes.

The spectrum of the TMA covered (H,OH)-Si(001) surface at 120 K (Figure 5 (b')) is usefully compared to that of the same system unfrozen at 300 K (Figure 5 (d')). Quantitative aspects are reported in Figure 6. After annealing, the TMA related losses decrease by ~90% while the SiO-H↔ loss recovers to ~94% of its initial peak area. This indicates that TMA adsorption via hydrogen-bonding is reversible for the majority species. Despite most molecules leave the surface upon annealing at 300 K, methyl modes (Figure 5(d')) are still observed at 300 K. The methyl region (345-377 meV) intensity represents (see Figure 5(a)) about 10% of the intensity seen for Q_{TMA}=1.5 ML at 120 K. It may be related to the aliphatic species detected by XPS if they can remain on the surface.

The spectra of (D,OD)-Si(001) exposed to TMA at 160 K and 105 K for various Q_{TMA} are shown in Figure 7(a). Difference spectra between successive TMA adsorption steps are given in Figure 7(b). As discussed before, the initial D_2O-covered surface presents the advantage of separating the methyl region from the O-D stretching mode, "unperturbed" and potentially

redshifted to lower energy. For the first exposure carried out at 160 K, see curves A and B in Figure 7(a) and the (gray-shaded) B-A difference curve in Figure 7(b), the intensity of the "unperturbed" O-D mode at 335 meV strongly decreases as TMA molecules stick on the surface (conversely the intensity of the $\nu(CH_3)$ mode at 360-370 meV, and the overtone/combination bands related to TMA in the 200-250 meV range increase). After addition of more TMA molecules at 160 K (curve C, and the red-shaded C-B difference curve) the surface coverage still increases (see the methyl region), and the "unperturbed" O-D peak still decreases. At 160 K, the gray-shaded difference spectrum curve in Figure 7(b) helps showing the appearance of two "bumps" at ~270 meV and ~308 meV. The former may correspond to the TMA(A) configuration (the rescaled calculated energy of TMA(A) is 271 meV, see Figure 7(c)), while the latter is less red-shifted, suggesting a weaker H-bonding. In any case, a strong, dominant O-D stretching peak centered at ~268 meV – practically the O-D stretching energy of the TMA(A) model – will only appear when the surface is cooled down to 105 K.

To ascertain whether TMA configurations different from the single-acceptor bond TMA(A) geometry (Figure 2(c)) are present on the surface, we need the support of theory. As already discussed in the XPS section 3.1, we must also consider double-acceptor configurations in "striped OH patterns" mimicked by the TMA(A,A) model of Figure 2(d). Our intuition was that, for a given TMA molecule, *weaker* hydrogen-bonds (leading to less red-shifted O-D modes) can be compensated by *more* hydrogen bonds, and thus that O-D stretching modes spanning the 271-335 meV interval could appear.

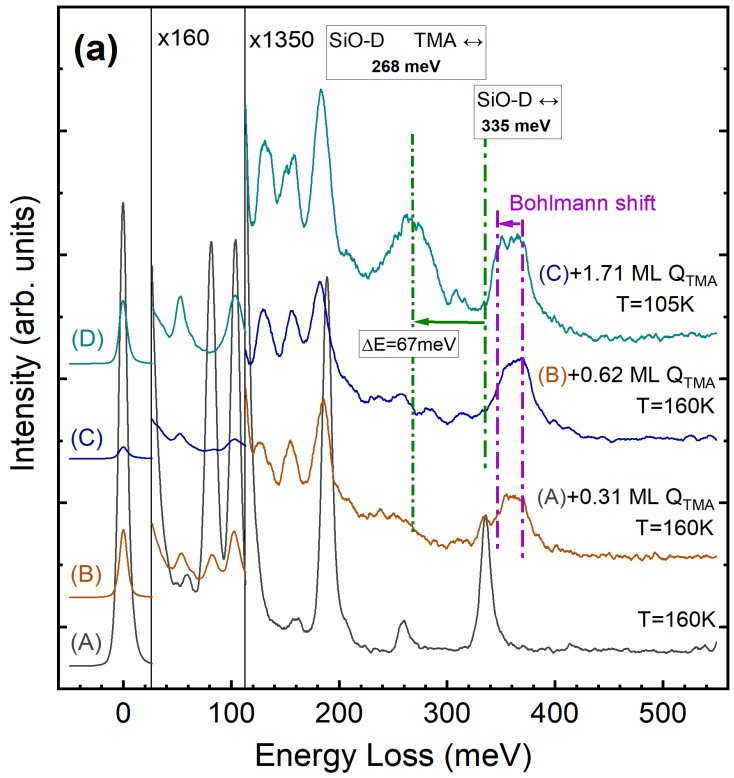
(a)
x160
x1350
SiO-D TMA ↔
268 meV
SiO-D ↔
335 meV
Bohlmann shift
(C)+1.71 ML Q_{TMA}
T=105K
ΔE=67meV
(B)+0.62 ML Q_{TMA}
T=160K
(A)+0.31 ML Q_{TMA}
T=160K
T=160K
(D)
(C)
(B)
(A)
Intensity (arb. units)
0
100
200
300
400
500
Energy Loss (meV)

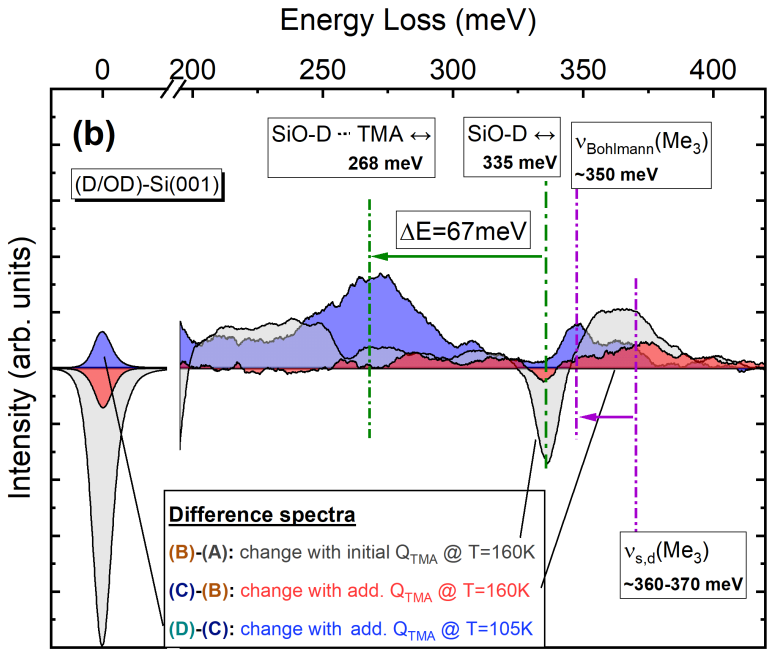
Energy Loss (meV)
0
200
250
300
350
400
(b)
(D/OD)-Si(001)
SiO-D ··· TMA ↔
268 meV
SiO-D ↔
335 meV
$\nu_{Bohlmann}(Me_3)$
~350 meV
ΔE=67meV
Intensity (arb. units)
Difference spectra
(B)-(A): change with initial Q_{TMA} @ T=160K
(C)-(B): change with add. Q_{TMA} @ T=160K
(D)-(C): change with add. Q_{TMA} @ T=105K
$\nu_{s,d}(Me_3)$
~360-370 meV

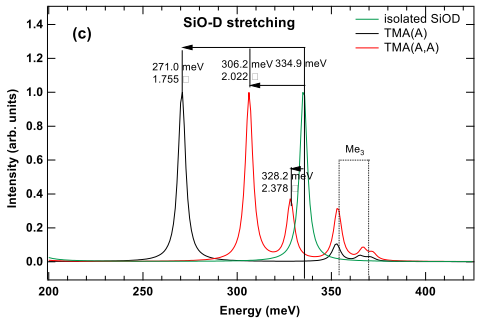

Figure 7. (a) Selected HREELS spectra of TMA adsorbed on (D,OD)-Si(001) at the indicated temperatures with increasing Q_{TMA} expressed in ML. (b) corresponding difference spectra in two selected energy loss regimes for TMA adsorption on (D,OD)-Si(001). The SiO-D redshift of ΔE=67 meV, highlighted in green, is due to the single acceptor hydrogen-bond formation between TMA and hydroxyls (TMA(A) configuration). The position of the Bohlmann band is indicated in purple. (c) DFT calculated vibrational spectra (energies are rescaled) for the free SiOD, the TMA(A) and the "striped pattern" TMA(A,A) in the methyl (Me_3) and SiO-D stretching region. Hydrogen-bond lengths are given. The maximum intensities of the SiO-D stretching modes are normalized to one. The vibration peaks are broadened by a Lorentzian of FWHM equal to 5 meV to help their visualization.

While the double hydrogen-bond has a weak impact on the N 1s ionization energy (see the XPS section 3.1), the SiO-D vibrational spectrum of the TMA(A,A) configuration is dramatically

different from that of the TMA(A) one, as shown in Figure 7(c). In fact, the hydrogen-bond lengths of TMA(A,A), 2.378 and 2.022 Å for the right and left hydrogen-bond in Figure 2(d), respectively, are both significantly longer than the single hydrogen-bond length of TMA(A), 1.755 Å. The rule "the shorter the hydrogen bond length the greater the O-H(D) redshift" applies (see also Table 2 for the correlation between hydrogen-bond lengths and O-H(D) distances). Figure 7(c) indicates that the two O-D stretching energies of the TMA(A,A) configuration are less redshifted with respect to the unperturbed SiOD case than the O-D mode of TMA(A). The longer hydrogen-bond (2.378 Å) corresponds to a SiO-D mode at 328 meV, a value close to that of the unperturbed SiO-D stretching mode (335 meV). For its part, the shorter hydrogen-bond (2.022 Å) corresponds to an O-D stretching peak shifted down to 306 meV. This value is halfway between that of the TMA(A) configuration and that of the unperturbed SiOD. It accounts for the bump at ~310 meV in the 160 K curve, that still remains as a clear shoulder in the 105 K curve. Situations of multiple hydrogen bonding can only be encountered at low coverage in patterns having adjacent OHs like the "striped pattern". Moreover, all the bonding possibilities on the "real" surface cannot be captured by the simple striped pattern two-dimer cluster we use, and one can expect redshifted contributions distributed between 271 and 335 meV. Only when saturation is reached (one TMA per OH) can the vibrational spectrum be "purified" by the dominance of the TMA(A) geometry. The methyl stretching region, including the Bohlmann band[49,50] at ~353 meV, is well reproduced by the calculation (compare Figure 7(c) to Figures 7(a,b)). In particular, the simulation shows that the nature of the hydrogen bond has no great impact on the methyl stretching components and their relative distribution.

On the basis of these vibration energy calculations, we can propose the following scenario to explain the spectroscopic observations relative to the O-D stretching mode, in particular the

temperature/coverage dependence. The ground-state DFT cluster calculation shows that when two adjacent OHs (in a "striped pattern") are available, the molecule prefers to adopt a double acceptor bond configuration. This shows that TMA(A,A) is more stable than TMA(A). Therefore, at 160 K, TMA(A,A) sites on "striped patterns" should be occupied first, being the lowest in energy. At this temperature, TMA(A) could also be found on "checkerboard patterns" (CBP in Figure 1) where the two OHs sit on Si atoms separated by 4.50 Å, a distance significantly longer than the Si-Si distance of 3.84 Å of the "striped pattern". As the TMA(A,A) configuration is more stable than the TMA(A) one on "striped patterns", to see it transformed into the TMA(A) configuration needs to decrease further the temperature to 105 K and increase the coverage up to saturation.

Calculated configuration	Si-O/Å	O-H/Å	N…H/Å
Unperturbed SiOD	1.692	0.961	NA
TMA(A)	1.663	0.997	1.755
TMA(A,A)			
- right*	1.692	0.966	2.378
- left*	1.675	0.978	2.022

Table 2. Si-O, O-H bond lengths and N…H hydrogen bond length calculated by DFT for the various configurations considered in this paper.*see Figure 2(c).

3.3 Hydrogen bonding and O-H bond weakening

The cluster DFT calculated bond lengths reported in Table 2 are relevant for a discussion on the catalytic role of TMA. It is clear that the shorter the hydrogen-bond length (N…H), the longer the O-H bond. Therefore the O-H bond is more weakened in the TMA(A) case than in the TMA(A,A) one. Multiple hydrogen-bonding between the tertiary amine and the surface OHs would negatively affect the activation of the O-H bond. This may explain why paired OHs may be less reactive with amino units than isolated OHs (see ref[12] and references therein).

The comparison of cluster DFT calculations of NH_3 in interaction with OHs also illustrates the effect of a difference in basicity. Single acceptor (A), single acceptor-single donor (A,D) and double-acceptor (A,A) geometries were calculated in ref[7]. The effect of an increased basicity from ammonia to TMA is only clear for the single acceptor hydrogen-bond, as the hydrogen bond length for NH_3(A) ("single dimer") and NH_3(A,D) ("striped pattern") is in the range 1.82-1.84 Å while it is significantly shorter, 1.76 Å, for TMA(A). However, this effect fades out for double acceptor bonds: the hydrogen bond lengths are 2.03/2.08 Å for NH_3(A,A) ("striped pattern") versus 2.02/2.38 Å for TMA(A,A).

4. Conclusion

Real-time synchrotron radiation XPS and HREELS were used in combination to determine the adsorption geometries of trimethylamine on the water-reacted (H,OH)-Si(001) surface at cryogenic temperatures. The paper highlights the complementarity of the two spectroscopic

techniques, and the effectiveness of DFT cluster calculations of core-level ionization and vibrational energies to interpret the results.

After adsorption of trimethylamine at 130 K on (H,OH)-Si(001) under ~3×10^{-9} mbar, real-time XPS detects the presence of three different adsorption configurations from the spectral decomposition of the N 1s spectra. The species are identified on the basis of calculated N 1s ionization energies. C 1s spectra are also used to give more insight on molecular dissociation and beam damage. One minority species is the TMA molecule datively bonded to an isolated dangling bond left after saturation of the surface by water (maximum coverage of ~0.04 ML). The datively bonded species tends to break down. This phenomenon occurs "in the dark", but it is clearly accelerated by exposure to the X-ray beam. The C 1s spectra analysis and time evolution points to different dissociation products when the beam is "off" or "on". The majority species is less firmly bonded to the surface than the minority ones (datively bonded and dissociated), as its coverage tends to diminish due to desorption once the reaction/analysis chamber is pumped down (the X-ray beam also helps the desorption of the molecule). This suggests that the majority species is hydrogen-bonded to the surface hydroxyls and calculated N 1s ionization energies are in good accord with this view.

For its part, HREELS clearly demonstrates that the surface hydroxyls are targeted by TMA, thus giving a definite proof of hydrogen bonding between TMA with surface hydroxyls. In fact, the intensity of the "unperturbed" O-H(D) stretching mode decreases with increasing TMA coverage. HREELS also shows that the adsorption geometry of the hydrogen-bonded molecules changes with temperature and coverage. The "proxy" is the O-H(D) stretching energy redshifted by the interaction with the amine. We took advantage of the fact that (H,OH)-Si(001) is one of the few surfaces with known OH patterns and we examined at the theoretical level the sites likely to

allow a multiple acceptor hydrogen bonding. Using a pair of OHs in a "striped pattern", we calculated that a double-acceptor bonding, TMA(A,A), leads to smaller O-H(D) redshifts than that resulting from a single-acceptor one, TMA(A). This provides an explanation for the observed changes, as double-acceptor bond geometry can form at low coverage, while at high coverage the single-acceptor bond geometry is predominant.

Considering that (H,OH)-Si(001) could be the starting surface in an ALD deposition process, the tertiary amine catalyst reacts with the electrically active surface defects (the isolated dangling bonds) with a likely impact on their density and thus on the band bending, and interacts with the hydroxyls. However, O-H bond activation certainly depends on the OH pattern itself and on the very nature of the acceptor hydrogen-bond, single versus double. The question of multiple acceptor bonds made by a tertiary amine in interaction with an OH pattern is new and also general, as it likely concerns those chemical reactions involving surface hydroxyls and their bonding with amino units on a great variety of OH-covered surfaces.

ASSOCIATED CONTENT

Supporting Information. The following file TMA_H_OH_Si (PDF) is available free of charge. It contains (i) the DFT simulation of vibrational spectra, (ii) a table of peak assignments from literature, and (iii) complementary Si 2p, O 1s and C 1s core-level.

AUTHOR INFORMATION

Corresponding Authors

*Jean-Jacques Gallet (jean-jacques.gallet@sorbonne-universite.fr)

*François Rochet (françois.rochet@sorbonne-universite.fr)

Present Addresses

† Now at Sorbonne Université, CNRS (UMR 8234), Physico-chimie des Electrolytes et Nanosystèmes Interfaciaux, 4 place Jussieu, 75252 Paris Cedex 05, France.

Author Contributions

The manuscript was written through contributions of all authors. All authors have given approval to the final version of the manuscript. ‡These authors contributed equally.

ACKNOWLEDGMENT

LPR thanks the "Ecole Doctorale" ED388 of Sorbonne Université for her PhD grant. Experiments were carried out with the approval of Sincrotrone ELETTRA, Italy.

ABBREVIATIONS

DFT density Functional Theory; IDB Isolated Dangling Bond; HREELS High Resolution Electron Energy Loss Spectroscopy; FWHM Full Width at Half Maximum; TMA Trimethylamine; STM Scanning Tunneling Microscopy; XPS X-ray Photoelectron Spectroscopy

REFERENCES

(1) Andersohn, L.; Köhler, U. In Situ Observation of Water Adsorption on Si(100) with Scanning Tunneling Microscopy. *Surf. Sci.* **1993**, *284* (1–2), 77–90. https://doi.org/10.1016/0039-6028(93)90526-P.

(2) Skliar, D. B.; Willis, B. G. The Role of Dangling Bonds in H2O-Induced Oxidation of Si(100)-2 × 1. *J. Phys. Chem. C* **2008**, *112* (25), 9434–9442. https://doi.org/10.1021/jp8010519.

(3) Gallet, J. J.; Bournel, F.; Rochet, F.; Köhler, U.; Kubsky, S.; Silly, M. G.; Sirotti, F.; Pierucci, D. Isolated Silicon Dangling Bonds on a Water-Saturated N+-Doped Si(001)-2 × 1 Surface: An XPS and STM Study. *J. Phys. Chem. C* **2011**, *115* (15), 7686–7693. https://doi.org/10.1021/jp201262x.

(4) Pierucci, D.; Gallet, J.-J.; Bournel, F.; Sirotti, F.; Silly, M. G.; Tissot, H.; Naitabdi, A.; Rochet, F. Real-Time X-Ray Photoemission Spectroscopy Study of Si(001)-2×1 Exposed to Water Vapor: Adsorption Kinetics, Fermi Level Positioning, and Electron Affinity Variations. *J. Phys. Chem. C* **2016**, *120* (38), 21631–21641. https://doi.org/10.1021/acs.jpcc.6b07360.

(5) Bournel, F.; Gallet, J.-J.; Köhler, U.; Ellakhmissi, B. B.; Kubsky, S.; Carniato, S.; Rochet, F. Propanoate Grafting on (H,OH)-Si(0 0 1)-2 × 1. *J. Phys. Condens. Matter* **2015**, *27* (5), 054005. https://doi.org/10.1088/0953-8984/27/5/054005.

(6) Pierucci, D.; Naitabdi, A.; Bournel, F.; Gallet, J.-J.; Tissot, H.; Carniato, S.; Rochet, F.; Köhler, U.; Laumann, D.; Kubsky, S.; Silly, M. G.; Sirotti, F. Benzaldehyde on Water-Saturated Si(001): Reaction with Isolated Silicon Dangling Bonds versus Concerted Hydrosilylation. *J. Phys. Chem. C* **2014**, *118* (19), 10005–10016. https://doi.org/10.1021/jp4077678.

(7) Pérez Ramírez, L.; Gallet, J. J.; Bournel, F.; Lim, F.; Carniato, S.; Rochet, F.; Yazyev, O. V.; Pasquarello, A.; Magnano, E.; Bondino, F. Hydrogen Bonding of Ammonia with (H,OH)-Si(001) Revealed by Experimental and Ab Initio Photoelectron Spectroscopy. *J. Phys. Chem. A* **2020**, *124* (26), 5378–5388. https://doi.org/10.1021/acs.jpca.0c03458.

(8) Longo, R. C.; Owen, J. H. G.; McDonnell, S.; Dick, D.; Ballard, J. B.; Randall, J. N.; Wallace, R. M.; Chabal, Y. J.; Cho, K. Toward Atomic-Scale Patterned Atomic Layer Deposition: Reactions of Al2O3 Precursors on a Si(001) Surface with Mixed Functionalizations. *J. Phys. Chem. C* **2016**, *120* (5), 2628–2641. https://doi.org/10.1021/acs.jpcc.5b09053.

(9) Dick, D.; Ballard, J. B.; Longo, R. C.; Randall, J. N.; Cho, K.; Chabal, Y. J. Toward Selective Ultra-High-Vacuum Atomic Layer Deposition of Metal Oxides on Si(100). *J. Phys. Chem. C* **2016**, *120* (42), 24213–24223. https://doi.org/10.1021/acs.jpcc.6b08130.

(10) Wilk, G. D.; Wallace, R. M.; Anthony, J. M. High-κ Gate Dielectrics: Current Status and Materials Properties Considerations. *J. Appl. Phys.* **2001**, *89* (10), 5243–5275. https://doi.org/10.1063/1.1361065.

(11) Chang, C.-Y.; Lin, C.-Y.; Lin, D.-S. How Dissociated Fragments of Multiatomic Molecules Saturate All Active Surface Sites—H2O Adsorption on the Si(100) Surface. *J. Phys. Condens. Matter* **2021**, *33* (40), 404004. https://doi.org/10.1088/1361-648X/ac14f7.

(12) Soethoudt, J.; Tomczak, Y.; Meynaerts, B.; Chan, B. T.; Delabie, A. Insight into Selective Surface Reactions of Dimethylamino-Trimethylsilane for Area-Selective Deposition of Metal, Nitride, and Oxide. *J. Phys. Chem. C* **2020**, *124* (13), 7163–7173. https://doi.org/10.1021/acs.jpcc.9b11270.

(13) Junige, M.; George, S. M. Area-Selective Molecular Layer Deposition of Nylon 6,2 Polyamide: Growth on Carbon and Inhibition on Silica. *J. Vac. Sci. Technol. A* **2021**, *39* (2), 023204. https://doi.org/10.1116/6.0000769.

(14) Klaus, J. W.; George, S. M. Atomic Layer Deposition of SiO2 at Room Temperature Using NH3-Catalyzed Sequential Surface Reactions. *Surf. Sci.* **2000**, *447* (1–3), 81–90. https://doi.org/10.1016/S0039-6028(99)01119-X.

(15) O'Neill, B. J.; Jackson, D. H. K.; Lee, J.; Canlas, C.; Stair, P. C.; Marshall, C. L.; Elam, J. W.; Kuech, T. F.; Dumesic, J. A.; Huber, G. W. Catalyst Design with Atomic Layer Deposition. *ACS Catal.* **2015**, *5* (3), 1804–1825. https://doi.org/10.1021/cs501862h.

(16) Fang, G.; Xu, L.; Ma, J.; Li, A. Theoretical Understanding of the Reaction Mechanism of SiO2 Atomic Layer Deposition. *Chem. Mater.* **2016**, *28* (5), 1247–1255. https://doi.org/10.1021/acs.chemmater.5b04422.

(17) Mayangsari, T. R.; Park, J.-M.; Yusup, L. L.; Gu, J.; Yoo, J.-H.; Kim, H.-D.; Lee, W.-J. Catalyzed Atomic Layer Deposition of Silicon Oxide at Ultralow Temperature Using Alkylamine. *Langmuir* **2018**, *34* (23), 6660–6669. https://doi.org/10.1021/acs.langmuir.8b00147.

(18) Kim, D. H.; Lee, H. J.; Jeong, H.; Shong, B.; Kim, W.-H.; Park, T. J. Thermal Atomic Layer Deposition of Device-Quality SiO 2 Thin Films under 100 °C Using an Aminodisilane Precursor. *Chem. Mater.* **2019**, *31* (15), 5502–5508. https://doi.org/10.1021/acs.chemmater.9b01107.

(19) Chen, S.; Fang, G.; Qian, X.; Li, A.; Ma, J. Influence of Alkalinity and Steric Hindrance of Lewis-Base Catalysts on Atomic Layer Deposition of SiO 2. *J. Phys. Chem. C* **2011**, *115* (47), 23363–23373. https://doi.org/10.1021/jp2048663.

(20) Fang, G.-Y.; Xu, L.-N.; Cao, Y.-Q.; Wang, L.-G.; Wu, D.; Li, A.-D. Self-Catalysis by

Aminosilanes and Strong Surface Oxidation by O 2 Plasma in Plasma-Enhanced Atomic Layer Deposition of High-Quality SiO 2. *Chem. Commun.* **2015**, *51* (7), 1341–1344. https://doi.org/10.1039/C4CC08004A.

(21) Hunter, E. P. L.; Lias, S. G. Evaluated Gas Phase Basicities and Proton Affinities of Molecules: An Update. *J. Phys. Chem. Ref. Data* **1998**, *27* (3), 413–656. https://doi.org/10.1063/1.556018.

(22) Gordon Group/GAMESS Homepage. Gordon Group/GAMESS Homepage http://www.msg.chem.iastate.edu/gamess/index.html (accessed Jun 7, 2013).

(23) Carniato, S.; Gallet, J.-J.; Rochet, F.; Dufour, G.; Bournel, F.; Rangan, S.; Verdini, A.; Floreano, L. Characterization of Hydroxyl Groups on Water-Reacted Si(001)-2×1 Using Synchrotron Radiation O 1s Core-Level Spectroscopies and Core-Excited State Density-Functional Calculations. *Phys. Rev. B* **2007**, *76* (8), 085321. https://doi.org/10.1103/PhysRevB.76.085321.

(24) Rangan, S.; Bournel, F.; Gallet, J.-J.; Kubsky, S.; Le Guen, K.; Dufour, G.; Rochet, F.; Sirotti, F.; Carniato, S.; Ilakovac, V. Experimental and Theoretical NEXAFS/XPS Study of the Room-Temperature Adsorption of Acetonitrile on Si(001)-2×1. *Phys. Rev. B* **2005**, *71* (16), 165319. https://doi.org/10.1103/PhysRevB.71.165319.

(25) Mathieu, C.; Bai, X.; Bournel, F.; Gallet, J.-J.; Carniato, S.; Rochet, F.; Sirotti, F.; Silly, M. G.; Chauvet, C.; Krizmancic, D.; Hennies, F. Nitrogen 1s NEXAFS and XPS Spectroscopy of NH3-Saturated Si(001)-2×1: Theoretical Predictions and Experimental Observations at 300 K. *Phys. Rev. B* **2009**, *79* (20), 205317. https://doi.org/10.1103/PhysRevB.79.205317.

(26) Mathieu, C.; Bai, X.; Gallet, J.-J.; Bournel, F.; Carniato, S.; Rochet, F.; Magnano, E.; Bondino, F.; Funke, R.; Köhler, U.; Kubsky, S. Molecular Staples on Si(001)-2 × 1: Dual-Head Primary Amines. *J. Phys. Chem. C* **2009**, *113* (26), 11336–11345. https://doi.org/10.1021/jp902918j.

(27) Jolly, W. L.; Bomben, K. D.; Eyermann, C. J. Core-Electron Binding Energies for Gaseous Atoms and Molecules. *At. Data Nucl. Data Tables* **1984**, *31* (3), 433–493. https://doi.org/10.1016/0092-640X(84)90011-1.

(28) Tautz, F. S.; Schaefer, J. a. Ultimate Resolution Electron Energy Loss Spectroscopy at H/Si(100) Surfaces. *J. Appl. Phys.* **1998**, *84* (12), 6636. https://doi.org/10.1063/1.369038.

(29) Polyakov, V.; Elbe, a; Wu, J.; Lapeyre, G.; Schaefer, J. Silicon Spreading in Delta -Doped GaAs(100): A High-Resolution Electron-Energy-Loss-Spectroscopy Study. *Phys. Rev. B. Condens. Matter* **1996**, *54* (3), 2010–2018.

(30) Hallac, B. F.; Asscher, M. The Chemistry of Trimethylamine on Ru(001) and O/Ru(001). *Langmuir* **2007**, *23* (17), 8891–8898. https://doi.org/10.1021/la700895r.

(31) DiLabio, G. A.; Dogel, S. A.; Wolkow, R. A. A Simple and Accurate Approach for Calculating the Vibration Spectra of Molecules on Surfaces: Comparisons to High Resolution Electron Energy Loss Data for Ethylene on Silicon. *Surf. Sci.* **2006**, *600* (16), L209–L213. https://doi.org/10.1016/j.susc.2006.05.057.

(32) Mulcahy, C. P. A.; Aquino, A. A.; Rogers, J. J.; Jones, T. S. Resonant Vibrational Excitation in High-Resolution Electron Energy-Loss Spectroscopy Studies of Trimethylamine Chemisorbed on GaAs(100). *J. Chem. Phys.* **1996**, *104* (22), 9120–9126.

https://doi.org/10.1063/1.471444.

(33) Ibach, H. *Electron Spectroscopy for Surface Analysis*; Springer Berlin Heidelberg, 1977.

(34) Cao, X.; Hamers, R. J. Silicon Surfaces as Electron Acceptors: Dative Bonding of Amines with Si(001) and Si(111) Surfaces. *J. Am. Chem. Soc.* **2001**, *123* (44), 10988–10996. https://doi.org/10.1021/ja0100322.

(35) Naitabdi, A.; Bournel, F.; Gallet, J.-J.; Markovits, A.; Rochet, F.; Borensztein, Y.; Silly, M. G.; Sirotti, F. Triethylamine on Si(001)-(2 × 1) at 300 K: Molecular Adsorption and Site Configurations Leading to Dissociation. *J. Phys. Chem. C* **2012**, *116* (31), 16473–16486. https://doi.org/10.1021/jp303002c.

(36) Dubey, G.; Rosei, F.; Lopinski, G. P. Molecular Modulation of Conductivity on H-Terminated Silicon-On-Insulator Substrates. *Small* **2010**, *6* (24), 2892–2899. https://doi.org/10.1002/smll.201001285.

(37) Tissot, H.; Gallet, J. J.; Bournel, F.; Pierucci, D.; Silly, M.; Sirotti, F.; Rochet, F. Dissociation of Ethoxysilane and Methoxysilane on Si(001)-2 × 1 and Si(111)-7 × 7 at Room Temperature: A Comparative Study Using Synchrotron Radiation Photoemission. *J. Phys. Chem. C* **2014**, *118* (42), 24397–24406. https://doi.org/10.1021/jp5050767.

(38) Naitabdi, A.; Rochet, F.; Carniato, S.; Bournel, F.; Gallet, J.-J. Room Temperature Differential Conductance Measurements of Triethylamine Molecules Adsorbed on Si(001). *Phys. Chem. Chem. Phys.* **2016**, *18* (33), 23231–23237. https://doi.org/10.1039/C6CP04350J.

(39) Mathieu, C.; Gallet, J.-J.; Bournel, F.; Rochet, F.; Bai, X.; Carniato, S.; Magnano, E.; Bondino, F.; Funke, R.; Köhler, U.; Kubsky, S. Molecular Staples on Si(001)-2 × 1: Dual-Head Primary Amines. *J. Phys. Chem. C 113* (26), 11336–11345. https://doi.org/10.1021/jp902918j.

(40) Barr, T. L.; Seal, S. Nature of the Use of Adventitious Carbon as a Binding Energy Standard. *J. Vac. Sci. Technol. A Vacuum, Surfaces, Film.* **1995**, *13* (3), 1239–1246. https://doi.org/10.1116/1.579868.

(41) Xu, J.; Choyke, W. J.; Yates, J. T. Role of the −SiH 3 Functional Group in Silane Adsorption and Dissociation on Si(100). *J. Phys. Chem. B* **1997**, *101* (35), 6879–6882. https://doi.org/10.1021/jp970832s.

(42) Reutzel, M.; Mette, G.; Stromberger, P.; Koert, U.; Dürr, M.; Höfer, U. Dissociative Adsorption of Diethyl Ether on Si(001) Studied by Means of Scanning Tunneling Microscopy and Photoelectron Spectroscopy. *J. Phys. Chem. C* **2015**, *119* (11), 6018–6023. https://doi.org/10.1021/jp511780p.

(43) Rochet, F.; Jolly, F.; Bournel, F.; Dufour, G.; Sirotti, F.; Cantin, J.-L. Ethylene on Si(001)-2×1 and Si(111)-7×7: X-Ray Photoemission Spectroscopy with Synchrotron Radiation. *Phys. Rev. B* **1998**, *58* (16), 11029–11042. https://doi.org/10.1103/PhysRevB.58.11029.

(44) Takeuchi, N.; Kanai, Y.; Selloni, A. Surface Reaction of Alkynes and Alkenes with H-Si(111): A Density Functional Theory Study. *J. Am. Chem. Soc.* **2004**, *126* (48), 15890–15896. https://doi.org/10.1021/ja046702w.

(45) Cicero, R. L.; Chidsey, C. E. D.; Lopinski, G. P.; Wayner, D. D. M.; Wolkow, R. A. Olefin

Additions on H−Si(111): Evidence for a Surface Chain Reaction Initiated at Isolated Dangling Bonds. *Langmuir* **2002**, *18* (2), 305–307. https://doi.org/10.1021/la010823h.

(46) Pitters, J. L.; Dogel, I.; DiLabio, G. A.; Wolkow, R. A. Linear Nanostructure Formation of Aldehydes by Self-Directed Growth on Hydrogen-Terminated Silicon(100). *J. Phys. Chem. B* **2006**, *110* (5), 2159–2163. https://doi.org/10.1021/jp055153t.

(47) Davies, B. M.; Craig, J. H. Electron-Beam-Induced Decomposition of Trimethylamine on Si(100)-2 × 1. *Surf. Interface Anal.* **2003**, *35* (13), 1060–1064. https://doi.org/10.1002/sia.1642.

(48) Lozano, J.; Early, D.; Craig, J. H.; Wang, P. W.; Kimberlin, K. R. HREELS, TPD and ESD Study of Electron-Induced Decomposition of Trimethylamine on Si(100) at 100 K. *Surf. Interface Anal.* **2005**, *37* (4), 366–373. https://doi.org/10.1002/sia.1990.

(49) Hossain, M. Z.; Machida, S.; Nagao, M.; Yamashita, Y.; Mukai, K.; Yoshinobu, J. Highly Selective Surface Lewis Acid−Base Reaction: Trimethylamine on Si(100)c(4×2). *J. Phys. Chem. B* **2004**, *108* (15), 4737–4742. https://doi.org/10.1021/jp037982p.

(50) Mui, C.; Wang, G. T.; Bent, S. F.; Musgrave, C. B. Reactions of Methylamines at the Si(100)-2×1 Surface. *J. Chem. Phys.* **2001**, *114* (22), 10170–10180. https://doi.org/10.1063/1.1370056.

(51) Kato, H. S.; Kawai, M.; Akagi, K.; Tsuneyuki, S. Interaction of Condensed Water Molecules with Hydroxyl and Hydrogen Groups on Si(001). *Surf. Sci.* **2005**, *587* (1–2), 34–40. https://doi.org/10.1016/j.susc.2005.04.032.

(1) Andersohn, L.; Köhler, U. In Situ Observation of Water Adsorption on Si(100) with Scanning Tunneling Microscopy. *Surf. Sci.* **1993**, *284* (1–2), 77–90. https://doi.org/10.1016/0039-6028(93)90526-P.

(2) Skliar, D. B.; Willis, B. G. The Role of Dangling Bonds in H2O-Induced Oxidation of Si(100)-2 × 1. *J. Phys. Chem. C* **2008**, *112* (25), 9434–9442. https://doi.org/10.1021/jp8010519.

(3) Gallet, J. J.; Bournel, F.; Rochet, F.; Köhler, U.; Kubsky, S.; Silly, M. G.; Sirotti, F.; Pierucci, D. Isolated Silicon Dangling Bonds on a Water-Saturated N+-Doped Si(001)-2 × 1 Surface: An XPS and STM Study. *J. Phys. Chem. C* **2011**, *115* (15), 7686–7693. https://doi.org/10.1021/jp201262x.

(4) Pierucci, D.; Gallet, J.-J.; Bournel, F.; Sirotti, F.; Silly, M. G.; Tissot, H.; Naitabdi, A.; Rochet, F. Real-Time X-Ray Photoemission Spectroscopy Study of Si(001)-2×1 Exposed to Water Vapor: Adsorption Kinetics, Fermi Level Positioning, and Electron Affinity Variations. *J. Phys. Chem. C* **2016**, *120* (38), 21631–21641. https://doi.org/10.1021/acs.jpcc.6b07360.

(5) Bournel, F.; Gallet, J.-J.; Köhler, U.; Ellakhmissi, B. B.; Kubsky, S.; Carniato, S.; Rochet, F. Propanoate Grafting on (H,OH)-Si(0 0 1)-2 × 1. *J. Phys. Condens. Matter* **2015**, *27* (5), 054005. https://doi.org/10.1088/0953-8984/27/5/054005.

(6) Pierucci, D.; Naitabdi, A.; Bournel, F.; Gallet, J.-J.; Tissot, H.; Carniato, S.; Rochet, F.; Köhler, U.; Laumann, D.; Kubsky, S.; Silly, M. G.; Sirotti, F. Benzaldehyde on Water-Saturated Si(001): Reaction with Isolated Silicon Dangling Bonds versus Concerted

Hydrosilylation. *J. Phys. Chem. C* **2014**, *118* (19), 10005–10016. https://doi.org/10.1021/jp4077678.

(7) Pérez Ramírez, L.; Gallet, J. J.; Bournel, F.; Lim, F.; Carniato, S.; Rochet, F.; Yazyev, O. V.; Pasquarello, A.; Magnano, E.; Bondino, F. Hydrogen Bonding of Ammonia with (H,OH)-Si(001) Revealed by Experimental and Ab Initio Photoelectron Spectroscopy. *J. Phys. Chem. A* **2020**, *124* (26), 5378–5388. https://doi.org/10.1021/acs.jpca.0c03458.

(8) Longo, R. C.; Owen, J. H. G.; McDonnell, S.; Dick, D.; Ballard, J. B.; Randall, J. N.; Wallace, R. M.; Chabal, Y. J.; Cho, K. Toward Atomic-Scale Patterned Atomic Layer Deposition: Reactions of Al2O3 Precursors on a Si(001) Surface with Mixed Functionalizations. *J. Phys. Chem. C* **2016**, *120* (5), 2628–2641. https://doi.org/10.1021/acs.jpcc.5b09053.

(9) Dick, D.; Ballard, J. B.; Longo, R. C.; Randall, J. N.; Cho, K.; Chabal, Y. J. Toward Selective Ultra-High-Vacuum Atomic Layer Deposition of Metal Oxides on Si(100). *J. Phys. Chem. C* **2016**, *120* (42), 24213–24223. https://doi.org/10.1021/acs.jpcc.6b08130.

(10) Wilk, G. D.; Wallace, R. M.; Anthony, J. M. High-κ Gate Dielectrics: Current Status and Materials Properties Considerations. *J. Appl. Phys.* **2001**, *89* (10), 5243–5275. https://doi.org/10.1063/1.1361065.

(11) Chang, C.-Y.; Lin, C.-Y.; Lin, D.-S. How Dissociated Fragments of Multiatomic Molecules Saturate All Active Surface Sites—H2O Adsorption on the Si(100) Surface. *J. Phys. Condens. Matter* **2021**, *33* (40), 404004. https://doi.org/10.1088/1361-648X/ac14f7.

(12) Soethoudt, J.; Tomczak, Y.; Meynaerts, B.; Chan, B. T.; Delabie, A. Insight into Selective

Surface Reactions of Dimethylamino-Trimethylsilane for Area-Selective Deposition of Metal, Nitride, and Oxide. *J. Phys. Chem. C* **2020**, *124* (13), 7163–7173. https://doi.org/10.1021/acs.jpcc.9b11270.

(13) Junige, M.; George, S. M. Area-Selective Molecular Layer Deposition of Nylon 6,2 Polyamide: Growth on Carbon and Inhibition on Silica. *J. Vac. Sci. Technol. A* **2021**, *39* (2), 023204. https://doi.org/10.1116/6.0000769.

(14) Klaus, J. W.; George, S. M. Atomic Layer Deposition of SiO2 at Room Temperature Using NH3-Catalyzed Sequential Surface Reactions. *Surf. Sci.* **2000**, *447* (1–3), 81–90. https://doi.org/10.1016/S0039-6028(99)01119-X.

(15) O'Neill, B. J.; Jackson, D. H. K.; Lee, J.; Canlas, C.; Stair, P. C.; Marshall, C. L.; Elam, J. W.; Kuech, T. F.; Dumesic, J. A.; Huber, G. W. Catalyst Design with Atomic Layer Deposition. *ACS Catal.* **2015**, *5* (3), 1804–1825. https://doi.org/10.1021/cs501862h.

(16) Fang, G.; Xu, L.; Ma, J.; Li, A. Theoretical Understanding of the Reaction Mechanism of SiO2 Atomic Layer Deposition. *Chem. Mater.* **2016**, *28* (5), 1247–1255. https://doi.org/10.1021/acs.chemmater.5b04422.

(17) Mayangsari, T. R.; Park, J.-M.; Yusup, L. L.; Gu, J.; Yoo, J.-H.; Kim, H.-D.; Lee, W.-J. Catalyzed Atomic Layer Deposition of Silicon Oxide at Ultralow Temperature Using Alkylamine. *Langmuir* **2018**, *34* (23), 6660–6669. https://doi.org/10.1021/acs.langmuir.8b00147.

(18) Kim, D. H.; Lee, H. J.; Jeong, H.; Shong, B.; Kim, W.-H.; Park, T. J. Thermal Atomic Layer Deposition of Device-Quality SiO 2 Thin Films under 100 °C Using an Aminodisilane

Precursor. *Chem. Mater.* **2019**, *31* (15), 5502–5508. https://doi.org/10.1021/acs.chemmater.9b01107.

(19) Chen, S.; Fang, G.; Qian, X.; Li, A.; Ma, J. Influence of Alkalinity and Steric Hindrance of Lewis-Base Catalysts on Atomic Layer Deposition of SiO 2. *J. Phys. Chem. C* **2011**, *115* (47), 23363–23373. https://doi.org/10.1021/jp2048663.

(20) Fang, G.-Y.; Xu, L.-N.; Cao, Y.-Q.; Wang, L.-G.; Wu, D.; Li, A.-D. Self-Catalysis by Aminosilanes and Strong Surface Oxidation by O 2 Plasma in Plasma-Enhanced Atomic Layer Deposition of High-Quality SiO 2. *Chem. Commun.* **2015**, *51* (7), 1341–1344. https://doi.org/10.1039/C4CC08004A.

(21) Hunter, E. P. L.; Lias, S. G. Evaluated Gas Phase Basicities and Proton Affinities of Molecules: An Update. *J. Phys. Chem. Ref. Data* **1998**, *27* (3), 413–656. https://doi.org/10.1063/1.556018.

(22) Gordon Group/GAMESS Homepage. Gordon Group/GAMESS Homepage http://www.msg.chem.iastate.edu/gamess/index.html (accessed Jun 7, 2013).

(23) Carniato, S.; Gallet, J.-J.; Rochet, F.; Dufour, G.; Bournel, F.; Rangan, S.; Verdini, A.; Floreano, L. Characterization of Hydroxyl Groups on Water-Reacted Si(001)-2×1 Using Synchrotron Radiation O 1s Core-Level Spectroscopies and Core-Excited State Density-Functional Calculations. *Phys. Rev. B* **2007**, *76* (8), 085321. https://doi.org/10.1103/PhysRevB.76.085321.

(24) Rangan, S.; Bournel, F.; Gallet, J.-J.; Kubsky, S.; Le Guen, K.; Dufour, G.; Rochet, F.; Sirotti, F.; Carniato, S.; Ilakovac, V. Experimental and Theoretical NEXAFS/XPS Study of

the Room-Temperature Adsorption of Acetonitrile on Si(001)-2×1. *Phys. Rev. B* **2005**, *71* (16), 165319. https://doi.org/10.1103/PhysRevB.71.165319.

(25) Mathieu, C.; Bai, X.; Bournel, F.; Gallet, J.-J.; Carniato, S.; Rochet, F.; Sirotti, F.; Silly, M. G.; Chauvet, C.; Krizmancic, D.; Hennies, F. Nitrogen 1s NEXAFS and XPS Spectroscopy of NH3-Saturated Si(001)-2×1: Theoretical Predictions and Experimental Observations at 300 K. *Phys. Rev. B* **2009**, *79* (20), 205317. https://doi.org/10.1103/PhysRevB.79.205317.

(26) Mathieu, C.; Bai, X.; Gallet, J.-J.; Bournel, F.; Carniato, S.; Rochet, F.; Magnano, E.; Bondino, F.; Funke, R.; Köhler, U.; Kubsky, S. Molecular Staples on Si(001)-2 × 1: Dual-Head Primary Amines. *J. Phys. Chem. C* **2009**, *113* (26), 11336–11345. https://doi.org/10.1021/jp902918j.

(27) Jolly, W. L.; Bomben, K. D.; Eyermann, C. J. Core-Electron Binding Energies for Gaseous Atoms and Molecules. *At. Data Nucl. Data Tables* **1984**, *31* (3), 433–493. https://doi.org/10.1016/0092-640X(84)90011-1.

(28) Tautz, F. S.; Schaefer, J. a. Ultimate Resolution Electron Energy Loss Spectroscopy at H/Si(100) Surfaces. *J. Appl. Phys.* **1998**, *84* (12), 6636. https://doi.org/10.1063/1.369038.

(29) Polyakov, V.; Elbe, a; Wu, J.; Lapeyre, G.; Schaefer, J. Silicon Spreading in Delta -Doped GaAs(100): A High-Resolution Electron-Energy-Loss-Spectroscopy Study. *Phys. Rev. B. Condens. Matter* **1996**, *54* (3), 2010–2018.

(30) Hallac, B. F.; Asscher, M. The Chemistry of Trimethylamine on Ru(001) and O/Ru(001). *Langmuir* **2007**, *23* (17), 8891–8898. https://doi.org/10.1021/la700895r.

(31) DiLabio, G. A.; Dogel, S. A.; Wolkow, R. A. A Simple and Accurate Approach for Calculating the Vibration Spectra of Molecules on Surfaces: Comparisons to High Resolution Electron Energy Loss Data for Ethylene on Silicon. *Surf. Sci.* **2006**, *600* (16), L209–L213. https://doi.org/10.1016/j.susc.2006.05.057.

(32) Mulcahy, C. P. A.; Aquino, A. A.; Rogers, J. J.; Jones, T. S. Resonant Vibrational Excitation in High-Resolution Electron Energy-Loss Spectroscopy Studies of Trimethylamine Chemisorbed on GaAs(100). *J. Chem. Phys.* **1996**, *104* (22), 9120–9126. https://doi.org/10.1063/1.471444.

(33) Ibach, H. *Electron Spectroscopy for Surface Analysis*; Springer Berlin Heidelberg, 1977.

(34) Cao, X.; Hamers, R. J. Silicon Surfaces as Electron Acceptors: Dative Bonding of Amines with Si(001) and Si(111) Surfaces. *J. Am. Chem. Soc.* **2001**, *123* (44), 10988–10996. https://doi.org/10.1021/ja0100322.

(35) Naitabdi, A.; Bournel, F.; Gallet, J.-J.; Markovits, A.; Rochet, F.; Borensztein, Y.; Silly, M. G.; Sirotti, F. Triethylamine on Si(001)-(2 × 1) at 300 K: Molecular Adsorption and Site Configurations Leading to Dissociation. *J. Phys. Chem. C* **2012**, *116* (31), 16473–16486. https://doi.org/10.1021/jp303002c.

(36) Dubey, G.; Rosei, F.; Lopinski, G. P. Molecular Modulation of Conductivity on H-Terminated Silicon-On-Insulator Substrates. *Small* **2010**, *6* (24), 2892–2899. https://doi.org/10.1002/smll.201001285.

(37) Tissot, H.; Gallet, J. J.; Bournel, F.; Pierucci, D.; Silly, M.; Sirotti, F.; Rochet, F. Dissociation of Ethoxysilane and Methoxysilane on Si(001)-2 × 1 and Si(111)-7 × 7 at

Room Temperature: A Comparative Study Using Synchrotron Radiation Photoemission. *J. Phys. Chem. C* **2014**, *118* (42), 24397–24406. https://doi.org/10.1021/jp5050767.

(38) Naitabdi, A.; Rochet, F.; Carniato, S.; Bournel, F.; Gallet, J.-J. Room Temperature Differential Conductance Measurements of Triethylamine Molecules Adsorbed on Si(001). *Phys. Chem. Chem. Phys.* **2016**, *18* (33), 23231–23237. https://doi.org/10.1039/C6CP04350J.

(39) Mathieu, C.; Gallet, J.-J.; Bournel, F.; Rochet, F.; Bai, X.; Carniato, S.; Magnano, E.; Bondino, F.; Funke, R.; Köhler, U.; Kubsky, S. Molecular Staples on Si(001)-2 × 1: Dual-Head Primary Amines. *J. Phys. Chem. C 113* (26), 11336–11345. https://doi.org/10.1021/jp902918j.

(40) Barr, T. L.; Seal, S. Nature of the Use of Adventitious Carbon as a Binding Energy Standard. *J. Vac. Sci. Technol. A Vacuum, Surfaces, Film.* **1995**, *13* (3), 1239–1246. https://doi.org/10.1116/1.579868.

(41) Xu, J.; Choyke, W. J.; Yates, J. T. Role of the −SiH 3 Functional Group in Silane Adsorption and Dissociation on Si(100). *J. Phys. Chem. B* **1997**, *101* (35), 6879–6882. https://doi.org/10.1021/jp970832s.

(42) Reutzel, M.; Mette, G.; Stromberger, P.; Koert, U.; Dürr, M.; Höfer, U. Dissociative Adsorption of Diethyl Ether on Si(001) Studied by Means of Scanning Tunneling Microscopy and Photoelectron Spectroscopy. *J. Phys. Chem. C* **2015**, *119* (11), 6018–6023. https://doi.org/10.1021/jp511780p.

(43) Rochet, F.; Jolly, F.; Bournel, F.; Dufour, G.; Sirotti, F.; Cantin, J.-L. Ethylene on Si(001)-

2×1 and Si(111)-7×7: X-Ray Photoemission Spectroscopy with Synchrotron Radiation. *Phys. Rev. B* **1998**, *58* (16), 11029–11042. https://doi.org/10.1103/PhysRevB.58.11029.

(44) Takeuchi, N.; Kanai, Y.; Selloni, A. Surface Reaction of Alkynes and Alkenes with H-Si(111): A Density Functional Theory Study. *J. Am. Chem. Soc.* **2004**, *126* (48), 15890–15896. https://doi.org/10.1021/ja046702w.

(45) Cicero, R. L.; Chidsey, C. E. D.; Lopinski, G. P.; Wayner, D. D. M.; Wolkow, R. A. Olefin Additions on H−Si(111): Evidence for a Surface Chain Reaction Initiated at Isolated Dangling Bonds. *Langmuir* **2002**, *18* (2), 305–307. https://doi.org/10.1021/la010823h.

(46) Pitters, J. L.; Dogel, I.; DiLabio, G. A.; Wolkow, R. A. Linear Nanostructure Formation of Aldehydes by Self-Directed Growth on Hydrogen-Terminated Silicon(100). *J. Phys. Chem. B* **2006**, *110* (5), 2159–2163. https://doi.org/10.1021/jp055153t.

(47) Davies, B. M.; Craig, J. H. Electron-Beam-Induced Decomposition of Trimethylamine on Si(100)-2 × 1. *Surf. Interface Anal.* **2003**, *35* (13), 1060–1064. https://doi.org/10.1002/sia.1642.

(48) Lozano, J.; Early, D.; Craig, J. H.; Wang, P. W.; Kimberlin, K. R. HREELS, TPD and ESD Study of Electron-Induced Decomposition of Trimethylamine on Si(100) at 100 K. *Surf. Interface Anal.* **2005**, *37* (4), 366–373. https://doi.org/10.1002/sia.1990.

(49) Hossain, M. Z.; Machida, S.; Nagao, M.; Yamashita, Y.; Mukai, K.; Yoshinobu, J. Highly Selective Surface Lewis Acid−Base Reaction: Trimethylamine on Si(100)c(4×2). *J. Phys. Chem. B* **2004**, *108* (15), 4737–4742. https://doi.org/10.1021/jp037982p.

(50) Mui, C.; Wang, G. T.; Bent, S. F.; Musgrave, C. B. Reactions of Methylamines at the Si(100)-2×1 Surface. *J. Chem. Phys.* **2001**, *114* (22), 10170–10180. https://doi.org/10.1063/1.1370056.

(51) Kato, H. S.; Kawai, M.; Akagi, K.; Tsuneyuki, S. Interaction of Condensed Water Molecules with Hydroxyl and Hydrogen Groups on Si(001). *Surf. Sci.* **2005**, *587* (1–2), 34–40. https://doi.org/10.1016/j.susc.2005.04.032.

Table of Contents